Accepted Manuscript

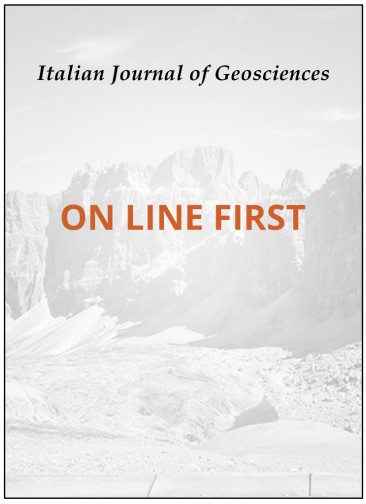

U–Pb ages on detrital zircons and geochemistry of Lula paragneiss from Variscan belt, NE Sardinia, Italy: implications for source rocks and early Paleozoic paleogeography

Gabriele Cruciani, Marcello Franceschelli, Valeria Caironi & Giovanni Musumeci

To appear in: *Italian Journal of Geosciences*

Received date: 20 June 2019

Accepted date: 23 September 2019

Doi: https://doi.org/10.3301/IJG.2019.24

Please cite this article as:

Cruciani G., Franceschelli M., Caironi V. & Musumeci G. - U–Pb ages on detrital zircons and geochemistry of Lula paragneiss from Variscan belt, NE Sardinia, Italy: implications for source rocks and early Paleozoic paleogeography. *Italian Journal of Geosciences*, https://doi.org/10.3301/IJG.2019.24

Ital. J. Geosci., Vol. 139 (2019), pp. 00, 14 Figs., 2 Tabs (https://doi.org/10.3301/IJG.2019.24)

U–Pb ages on detrital zircons and geochemistry of Lula paragneiss from Variscan belt, NE Sardinia, Italy: implications for source rocks and early Paleozoic paleogeography

Gabriele Cruciani (1), Marcello Franceschelli (1), Valeria Caironi (2) & Giovanni Musumeci (3)

ABSTRACT

Chemical analyses of garnet-bearing metasediments and EMP and U/Pb analyses of detrital zircons of the Lula paragneisses in the Axial Zone of Variscan belt (NE Sardinia) give significant contribution to the reconstruction of the early Paleozoic evolution of northern Gondwana margin. The youngest middle Ordovician (465 Ma) age of detrital zircons indicate a derivation from a fore-arc sedimentary basin along an early Paleozoic convergent margin, which collected sediments from nearby emerged lands consisting of early Paleozoic volcanic arcs and pre-Paleozoic sequences. The chemical composition of metasediments is characterized by negative Sr anomaly and depletion in heavy rare earth elements (HREE) and Y as compared to the upper crust. Normalized to chondrite values, the paragneiss shows a steep REE pattern with light-REE enrichment, negative Eu anomaly and flat heavy-REE pattern. All these features suggest a derivation form older active continental margins or island arcs. Detrital zircon ages cover a very large time span (3151 + 97 Ma to 465 + 8 Ma) and reveal a complex history of inheritance and recycling. The oldest ages obtained on relic cores and/or magmatic stages, mostly enriched in Hf (Zr / Hf ratios: 45-24) and devoid of Y, indicate a contribution from granitoid rocks of mainly crustal origin. The ages of detrital zircons highlight a derivation from the sedimentary supply from the Sahara craton and/or the Arabian-Numidian shield along the northeastern margin of Gondwana. This fit well with derivation of early Paleozoic metasedimentary formations in southern Sardinia and northern Apennine, pointing out a common origin and location of these sedimentary basins along the northern margin of Gondwana at the early Paleozoic. As regards the Variscan orogeny, the common middle Ordovician age of Lula paragneiss and nearby Lodé orthogneiss highlight the role of Variscan tectonics in the assembly of different blocks of early-middle Paleozoic margin.

Key Words: *U-Pb zircon geochronology, paragneiss, geochemistry, Variscan Sardinia.*

INTRODUCTION

Large parts of southern Europe Variscan chain derive from the so called peri-Gondwanan terranes, a mosaic of continental blocks that were rifted away from the northern Gondwana margin as a consequence of the opening of the Rheic Ocean in the Early Ordovician (Avigad *et* alii, 2012 and reference therein). Some of these terranes (i.e. Sardinia Block, Mid Armorican Domain, Pyrenees) experienced early to middle-late Ordovician magmatism, respectively related to the opening of Rheic Ocean (Murphy *et* alii, 2006; Nance *et alii*, 2010) and to an Andean-type volcanic arc and/or subduction-accretion margin (Oggiano *et alii*, 2010; Cruciani *et alii*, 2019a). In some places deposition of clastic sedimentary sequences was coeval with Ordovician magmatism. The current level of erosion exposes large volumes of low to medium-high grade metamorphic rocks (i.e. metavolcanic, metarkose, metasandstone, orthogneiss, paragneiss) derived from middle-late Ordovician magmatic or sedimentary rocks from inner to the outer zones of the Variscan chain. Thus, these rocks, and their geochemical composition, represent very important records of geological history that allow to better understand the evolution of Gondwana, and peri-Gondwanan terranes at that time (Fernandez - Suarez *et alii*, 2000; Trombetta *et alii*, 2004; Avigad *et alii*, 2012).

In order to reconstruct the Early Paleozoic evolution of the Sardinian block and give additional data for paleogeographic reconstructions of peri-Gondwanan terranes, we have undertaken a geochemical and radiometric study of paragneisses (Lula paragneiss) exposed in the inner zone of the Variscan belt in NE Sardinia. Such rocks have been regarded as the host rocks of middle Ordovician granitoids (Lodé-Mamone orthogneiss; Carmignani *et alii*, 1994 and reference therein). The geochemical and radiometric data allow to shed some ligth on the origin of the Lula paragneiss and on the tectonic setting of sedimentary basins and acidic magmatism in the Early Paleozoic. Moreover, on the basis of detrital zircon ages, a comparison with other Early Paleozoic clastic sequences in Sardinia and northern Apennine Paleozoic basement allows to make some considerations about the paleogeographic reconstruction of these peri-Gondwanan terranes at the early Paleozoic time.

GEOLOGICAL FRAMEWORK

The Sardinian basement consists of Cambrian to Lower Carboniferous metamorphic sequences and Late Carboniferous to Permian igneous rocks, in turn covered by Carboniferous-Permian sedimentary rocks and Permian volcanics (Carmignani *et alii*, 1994, 2001; Barca *et alii*, 1995). Since the 90ties, the Sardinian metamorphic basement was classically subdivided into the following four tectono-metamorphic zones from SW to NE (Fig. 1a):

(1) Dipartimento di Scienze Chimiche e Geologiche, Università degli Studi di Cagliari, S.S. 554 Cittadella Universitaria, Monserrato (CA), 09042, Italy
(2) Dipartimento di Scienze della Terra "Ardito Desio" Università degli Studi di Milano, via Botticelli 23, 20133 Milano
(3) Dipartimento di Scienze della Terra, Università degli Studi di Pisa, Via Santa Maria 53, I-56126, Pisa, Italy
Corresponding author e-mail: gcrucian@unica.it

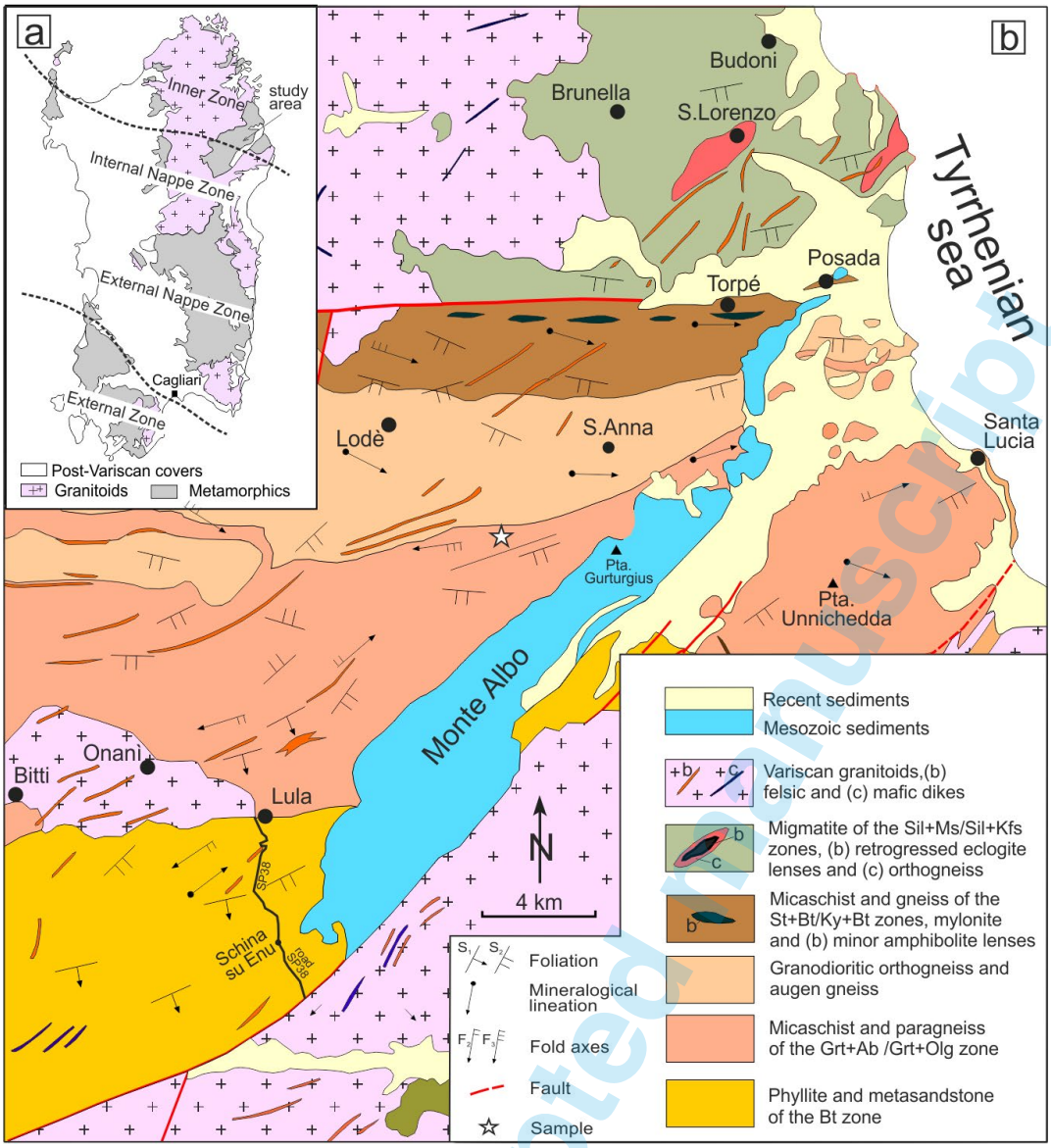

Fig. 1 - a) simplified tectonic sketch map of the Variscan Sardinian chain (the arrow refers to the study area shown in detail in b); b) geological sketch map of the NE Sardinia metamorphic basement in the Lula area. The localization of the studied samples is also shown. Modified from Cruciani *et alii* (2013b).

1) the External Zone (South-western Sardinia), 2) the External Nappe Zone (Central to Southern Sardinia), 3) the Internal Nappe Zone (Northern to Central Sardinia), and 4) the Inner or Axial Zone (Northern Sardinia and Southern Corsica) (Carmignani *et alii*, 2001; Rossi *et alii*, 2009; Massonne *et alii*, 2018).

The External Zone, in southern Sulcis, consists of a Cambro-Ordovician sequence that, from bottom to top, includes the Mt. Filau orthogneiss, Monte Settiballas schists and Bithia Unit (Pavanetto *et alii*, 2102; Costamagna *et alii*, 2016; Cruciani *et alii*, 2019a). In the Iglesiente, the Paleozoic sequence is composed of the Cambrian siliciclastic to carbonate deposits of the Nebida, Gonnesa and Iglesias Group (Pillola *et alii*, 1995) separated by the Sardic unconformity from the overlying siliciclastic sequence related to the sinking of the passive margin (Leone *et alii*, 1991), whose age is Late Ordovician to Early Carboniferous.

The Nappe Zone, in turn subdived into Internal and External Nappe Zone, results from southward thrusting with km-scale isoclinal folding and syntectonic regional metamorphism ranging from lower greenschist to amphibolite facies conditions (Carmignani *et alii*, 1994; Cruciani *et alii*, 2016). The lithostratigraphic successions in the Nappe Zone consist of Late Cambrian to Early Carboniferous metasedimentary rocks with Middle–Upper Ordovician and Early Silurian calc-alkaline (Oggiano *et alii*, 2010; Cruciani *et alii*, 2013a; Musumeci *et alii*, 2015) and alkaline meta-igneous rocks. In the External Nappe Zone crops out a thick Middle to Late Ordovician volcano-sedimentary to epiclastic succession arranged into a southward verging stack of allochthonous nappes (Conti *et alii*, 2001): Monte Grighini Unit, Rio Gruppa - Castello Medusa Unit, Gerrei Unit, Meana Sardo Unit, Sarrabus Unit and Arburese Unit.

The Inner Zone is formed by two metamorphic complexes: i) the Low- to Medium-Grade Metamorphic Complex (L-MGMC): micaschists (locally with HP metamorphic overprint, Cruciani *et alii*, 2013b), paragneisses and orthogneisses reaching amphibolite-facies conditions; ii) the High-Grade Metamorphic Complex (HGMC, or Migmatite Complex): mainly igneous

and sedimentary-derived migmatites (Massonne *et alii*, 2013; Cruciani *et alii*, 2014a,b; Fancello *et alii*, 2018) embedding metabasite lenses with relics of granulites (Scodina *et alii*, 2019) and eclogites (Franceschelli *et alii*, 2007; Cruciani *et alii*, 2019b). The L-MGMC also contains eclogite-facies metabasite (Cruciani *et alii*, 2010, 2011, 2015a,b) and amphibolite lenses in the Posada Valley. A Variscan transpressive shear belt (Carosi & Palmeri, 2002; Iacopini *et alii*, 2008; Carosi *et alii*, 2009) marks the boundary between HGMC and L-MGMC and is easily recognizable along the Posada Valley, in southern Gallura, and within Asinara Island (Oggiano & Di Pisa, 1992; Carosi *et alii*, 2004; 2005; 2009).

GEOLOGICAL OUTLINE OF NE SARDINIA

A geological sketch map of the study area is shown in Fig. 1b (from Costamagna *et alii*, 2012). From south to north, the following litothypes have been distinguished: 1. phyllite and metasandstone of the biotite zone; 2. micaschist and paragneiss with garnet (+albite/oligoclase); 3. granodioritic orthogneiss and augen gneiss; 4. micaschist and paragneiss with staurolite+biotite and kyanite+biotite, mostly mylonitic; 5. gneiss and migmatite (with minor calcsilicate rocks) containing amphibolite lenses that preserve granulite and eclogite facies relics; 6. granitoids belonging to the Variscan batholith. According to Carmignani *et alii* (2001), litothype 1 belongs to the Nappe Zone, while lithotypes from 2 to 6 belong the to the Axial Zone. The transition from the northern Internal Nappe Zone to the L-MGMC occurs close to Lula: it is marked by the appearance of mm-sized garnet crystals and by the disappearance of any relic of sedimentary features which are instead observed in the metasandstones (Costamagna *et alii*, 2012). The L-MGMC is formed by ortho- and paragneisses with well developed schistosity and thinly foliated micaschists. According to Costamagna *et alii* (2012), these rocks may derive from acidic and intermediate volcanics, arkosic sandstones and carbonaceous pelites: this is in good agreement with the Middle Ordovician to Silurian protolith stratigraphy of the Variscan anchimetamorphic areas of Southern Sardinia (Pavanetto *et alii*, 2012; Cruciani *et alii* 2018). U–Pb zircon dating of meta-igneous rocks (Lula porphyroid) enclosed in the phyllites gives an age of 474 ± 13 Ma (Helbing & Tiepolo, 2005).

At the transition between the Internal Nappes and the Inner Zone (Fig.1), the metamorphic grade increases over a distance of about 40 km from the biotite to the sillimanite + K-feldspar zone. Metamorphic zoning of pelitic sequences from NE Sardinia (Fig. 1), based on the regional distribution of AFM minerals, was described by Franceschelli *et alii* (1982, 1989) and Connolly *et alii* (1994) and consists, from south to north, of the following six metamorphic zones: 1) biotite, 2) garnet, 3) staurolite + biotite, 4) kyanite + biotite, 5) sillimanite + muscovite, 6) sillimanite + K-feldspar. P-T path of the rocks from NE Sardinia can be found in Franceschelli *et alii* (1989), Connolly *et alii* (1994); Ricci *et alii* (2004), Cruciani *et alii* (2015c).

In NE Sardinia, a polyphase deformation was described by Franceschelli *et alii* (1982), Carmignani *et alii* (1994), Connolly *et alii* (1994), Carosi *et alii* (2005) and Helbing *et alii* (2006). The D_1 collision-related deformation is well-recorded in the L-MGMC, where it is associated with a penetrative S_1 axial plane foliation of SW-facing folds. Late D_1 ductile/brittle shear zones, with top to the SW sense of movement, overprint F_1 folds. Towards north the S_1 foliation is progressively transposed by the D_2 phase, which is associated with upright up to NE verging folds and dextral shear zones. The Variscan D_2 transpressive shear belt (Carmignani *et alii*, 1994) that separates the HGMC from L-MGMC is related to the NNE-SSW compression and NW-SE shear displacement (Carosi & Palmeri, 2002; Iacopini *et alii*, 2008; Carosi *et alii*, 2009).

A D_3 deformation phase forming upright metric to decametric open folds developed subsequently. F_3 folds are associated with an S_3 axial plane crenulation cleavage. The D_4 tectonic phase is revealed by metric to decametric folds with sub-horizontal axial planes (Cruciani *et alii*, 2015c).

Neighbouring chloritoid schist investigated by Cruciani *et alii* (2013b) north of the Lula village suggest an HP-metamorphic imprint at pressures close to 1.8 GPa and temperatures of 460–500 °C followed by amphibolite-facies re-equilibration (540–570 °C and 0.7–1.0 GPa).

ANALYTICAL METHODS

Major elements, trace and rare earth elements (REE) of whole rock samples were determined at the ALS-Chemex Laboratories, Seville, Spain. Mineral chemistry on albite, garnet, white mica, and chlorite were performed with a FEI Quanta 200 SEM equipped with an EDAX-EDS detector at CeSAR, Centro Servizi d'Ateneo per la Ricerca, Università di Cagliari. Zircons were separated with conventional methods (crushing with hydraulic press, heavy liquids, magnetic separation, hand picking). Some zircon crystals that during magnetic separation (Frantz isodynamic magnetic separator) were attracted at the positive pole at the maximum intensity (1.75 A) were separately mounted and labelled as sample B, whereas the non-magnetic crystals are indicated as sample A. Zircons were then mounted in epoxy resin, abraded to expose the internal zones, polished and characterized for the internal structure by cathodoluminescence (CL). They were analyzed for Si, Zr, Hf, Y, P, U and Th by EMP (Jeol JXA-8200) at the Earth Science Department of the University of Milan. In-situ U-Pb geochronology was carried out with an excimer laser ablation (ELA)-ICPMS at C.N.R.-I.G.G.-U.O.S. of Pavia. The laser ablation system couples a 193 nm ArF excimer laser microprobe (Geolas200Q-Microlas) with a ICPMS Element I from Thermo Finnigan. The analytical method is basically that described in Tiepolo (2003). Instrumental and laser-induced U/Pb fractionations were corrected using as external standard zircon GJ-1 (Jackson *et alii*, 2004). The same integration intervals and spot size were used on both the external standard and unknowns. During each analytical run reference zircon 02123 (Ketchum *et alii*, 2001) or 91500 (Wiedenbeck *et alii*, 1995) were analysed together with unknowns for quality control. The spot size was set to 20 μm, 5Hz of repetition rate and 12J/cm^2 as laser fluency. Data reduction was carried out using the "Glitter" software package (van Achterbergh *et alii*, 2001). During each analytical run the reproducibility on the standards was propagated to all determinations. Concordia ages were determined and Concordia plots were constructed using the Isoplot/EX 3.0 software (Ludwig, 2000). All errors in the text are given at 2s level.

PETROGRAPHY

The studied samples of Lula paragneiss (Fig. 2a) come from the upper part of the garnet zone, not far from the contact with the granodioritic orthogneiss and augen gneiss (sample location is shown in Fig. 1b). The Lula paragneiss is characterized by a gneissic fabric with quartz-feldspathic layers alternating with mica-rich layers (Fig. 2b). The paragneiss consists of quartz, albite porphyroblasts, K-white mica, biotite, garnet, late chlorite and accessory apatite, zircon, and Fe-oxides. Among the different samples a significant variation in grain size as well as in the albite/mica ratio can be observed. Albite (X_{Na} > 0.98) porphyroblasts are embedded in a lepidoblastic matrix consisting of K-white mica, chlorite and chloritized biotite. The porphyroblasts are surrounded at their boundaries by pressure shadows, mainly consisting of K-white mica, chlorite and/or recrystallized quartz. Chlorite in the rock matrix has X_{Mg} ratio ~ 0.27. The albite porphyroblasts also contain elongated and slightly oriented inclusions, mainly made up of white mica, quartz and opaque minerals, which identify an old S1 foliation. Armored white mica relicts in albite have X_{Mg}: 0.4-0.5 and Si: 6.7-6.8 a.p.f.u. (on the basis of 22 oxygens). S_1 is also preserved as a relict foliation within microlithons in the lepidoblastic layers. The lepidoblastic layers consist of a close association of K-white mica flakes forming elongated trails together with subordinate biotite and chlorite. The white mica from these trails shows X_{Mg}: 040-0.46 and Si: 6.2 – 6.7 a.p.f.u.. The S_2 schistosity, which is the pervasive rock foliation subparallel to the compositional layering, is marked by the alignment of K-white mica and subordinate biotite as well as by the rough orientation of elongated albite porphyroblasts. However, some albite porphyroblasts forming a slight angle with S_2 schistosity indicate that albite is pre- to synkinematic with respect to D_2 deformation. In the quartz-feldsphatic layers, quartz recrystallization is commonly observed. In the studied samples garnet occurs as small, submillimetric euhedral to subheudral crystals with a composition ranging within the following values: Alm_{65-68} Prp_{1-2} Sps_{9-12} Grs_{20-21}. Moving from south to north of the investigated area, a progressive overprint of the S_2 foliation over the S_1 has been observed. Locally, the S_2 foliation is gently folded by a further deformation (D_3).

GEOCHEMISTRY

Major and trace element composition of some selected paragneiss samples from the garnet zone of Lula area is given in Table 1. Most of the samples (n. 8 samples out of ten) are within the following compositional range (wt.%): SiO_2 67.3-76.5, Al_2O_3 12-16, Fe_2O_{3tot} 2.8-4.8, MgO 0.8-1.6, K_2O 1.7-3.7, Na_2O 1.2-3.4. Two samples (L218, L222) are characterized by higher SiO_2 (~86-89 wt.%) and lower contents of Al_2O_3 (5.4-6.7), Fe_2O_{3tot} (1.4-2.3), MgO (<0.6), Na_2O (~0.1) and K_2O (1.3-1.7). P_2O_5 is very low in these latter samples (0.03wt.% in L218, 0.04 in L222) recording a significantly lower apatite content as compared to the other samples. In the $Log(SiO_2/Al_2O_3)$ vs. $Log(Fe_2O_3/K_2O)$ diagram after Herron (1988) shown in Fig. 3, most samples plot in the wacke field, very near to the Lula metasandstones of Costamagna *et alii* (2012). Samples L218 and L222, due to their higher SiO_2 content, plot in the sublitharenite field.

Strong positive correlations of the major oxides with Al_2O_3 suggest that they are mostly associated with phyllosilicate content. The Na_2O and K_2O depletion in samples L218, L222 as compared to the other samples is consistent with their relatively lower feldspar and higher quartz content. The K_2O/Na_2O ratio is <1 for six samples out of ten, slightly higher for L66 (2.31) and L214 (2.23), whereas it is >> 1 in samples L218, L222 (K_2O/Na_2O: 7.6 and 17.6, respectively) in agreement with the decrease in albite and increase in K-bearing minerals observed from the first to the latter group.

Trace and rare earth elements

The trace element spider diagrams for the Lula paragneiss (this study) and for the Lula metasandstones from Costamagna *et alii* (2012), normalized to the composition of upper crust (according to Rudnick & Fountain, 1995), are shown in Fig. 4a.

Fig. 2 - a) Field aspect of Lula paragneiss; b) hand specimen sample L214 of Lula paragneiss; for sample location see Fig. 1.

TABLE 1

Major element (wt%) and trace element (ppm) of selected samples of Lula paragneiss.

	L18	**L19**	**L 66**	**L 214**	**L 216**	**L 225**	**L 215**	**L 223**	**L 218**	**L 222**
SiO_2	71.58	69.18	67.31	76.57	71.93	71.33	72.9	71.87	89.62	86.81
TiO_2	0.61	0.66	0.79	0.73	0.56	0.67	0.56	0.63	0.42	0.48
Al_2O_3	13.59	15.2	16.42	12.62	13.28	13.49	12.92	13.45	5.45	6.75
Fe_2O_{3tot}	4.53	4.55	4.79	2.79	4.26	4.64	4.34	4.23	1.39	2.34
MnO	0.04	0.05	0.02	0.01	0.05	0.06	0.04	0.04	0.01	0.02
MgO	1.38	1.49	1.16	0.78	1.4	1.6	1.33	1.38	0.31	0.54
CaO	0.54	0.83	0.1	0.04	0.53	0.93	0.59	0.48	0.05	0.03
Na_2O	2.85	2.93	1.62	1.28	3.44	3.31	3.14	3.28	0.17	0.1
K2O	1.82	2.61	3.75	2.85	2.52	1.76	2.37	2.04	1.3	1.76
P_2O_5	0.13	0.13	0.08	0.06	0.15	0.2	0.16	0.16	0.03	0.04
LOI	2.63	2.52	3.63	2.32	1.92	2.11	1.54	1.96	1.16	1.37
Total	99.70	100.15	99.67	100.05	100.04	100.10	99.89	99.52	99.91	100.24
Li	50	30	50	30	20	40	30	30	20	20
Sc	9	10	12	8	9	10	8	9	3	4
V	72	88	94	66	65	76	71	73	26	37
Cr	60	70	60	40	50	60	60	210	220	20
Co	9	12	14	8	7	10	9	8	2	3
Ni	27	31	28	20	23	25	24	26	8	13
Cu	63	28	22	29	21	30	44	69	169	16
Zn	58	77	76	30	47	66	57	50	18	42
Ga	18.7	23.4	22.6	18.3	16.3	18.2	18.3	17.8	8	9.9
As	30	8	10	6	<5	<5	12	5	8	6
Rb	62.6	109.5	123	90.2	109	63.1	88.3	77.1	48	71.1
Sr	124.5	148	78	53.5	156.5	164	130	124	23.3	30.7
Y	22.2	31.4	23.3	20.8	14.3	25.9	22.3	20.3	12.7	18.9
Zr	242	258	265	474	232	280	206	237	417	488
Nb	11.2	12.6	15.5	12.7	10.9	11.5	10.8	11.5	8	10.2
Sn	2	4	3	2	2	3	4	3	2	2
Cs	1.18	4.05	3.00	2.19	1.43	1.00	1.20	1.43	1.28	1.44
Ba	440	591	833	679	296	476	581	478	258	312
Hf	6.6	6.8	6.8	12.3	6.4	6.7	5.7	6.1	9.8	11.8
Ta	0.9	1.0	1.2	0.9	0.9	0.8	0.8	0.9	0.7	0.7
W	2	2	2	1	1	1	2	2	2	3
Pb	23	26	17	11	19	18	56	21	29	29
Th	10.8	12.65	12.5	13.1	11.35	10.95	10.9	10.8	8.55	9.8
U	2.63	4.91	3.16	3.37	2.15	2.44	1.9	1.9	2.39	2.31
La	28.2	45.9	39.4	33.2	16.6	20.7	34.7	16.3	19.3	28.9
Ce	46.5	73.1	86.2	67.3	42.6	39.7	63.2	19.8	37.9	59
Pr	6.70	10.0	9.30	7.68	4.02	5.08	7.90	3.78	4.41	6.48
Nd	24.9	37.5	34.0	28.3	14.8	19.7	29.7	15.9	16.1	24.5
Sm	5.03	6.68	6.65	4.86	2.84	4.26	5.5	2.97	2.92	4.32
Eu	1.23	1.47	1.34	1.18	0.76	0.82	1.12	0.71	0.63	1.05
Gd	4.38	6.42	5.38	4.23	2.46	4.37	5.4	3.16	2.67	4.06
Tb	0.65	0.91	0.66	0.63	0.43	0.68	0.73	0.52	0.37	0.59
Dy	4.04	5.78	4.30	3.89	2.79	4.57	4.58	3.23	2.05	3.45
Ho	0.81	1.08	0.86	0.74	0.55	0.93	0.85	0.69	0.46	0.66
Er	2.48	3.03	2.50	2.53	1.85	2.74	2.47	2.31	1.36	2.06
Tm	0.34	0.45	0.37	0.32	0.28	0.43	0.36	0.35	0.19	0.32
Yb	2.21	2.62	2.35	2.4	1.63	2.7	2.23	2.00	1.44	1.83
Lu	0.34	0.44	0.37	0.37	0.24	0.38	0.33	0.30	0.21	0.32

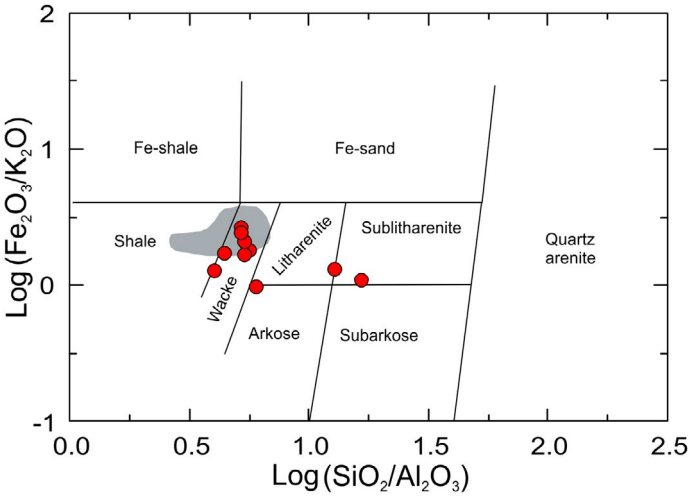

Fig. 3 - Log(SiO_2/Al_2O_3) vs. Log(Fe_2O_3/K_2O) classificative diagram after Herron (1988) of Lula paragneiss. The grey area shows the compositional range of the Lula metasandstones reported by Costamagna *et alii* (2012).

The studied samples are characterized by a marked negative anomaly for Sr and are slightly depleted in heavy rare earth elements (such as Er, Yb, Lu) and Y as compared to the upper crust. Among the large ion lithophile elements (LILE), Th shows very good correlation with Al_2O_3 (r: 0.81) and with TiO_2 (0.88), suggesting that its distribution is mainly controlled by biotite and/or by other mafic minerals. The Th/U ratio of the samples is comprised between 2.6 -5.7 (average: 4.4) indicating that the paragneiss are fresh, not weathered samples (Bakkiaraj *et alii*, 2010). Rb, Sr, Ba are also positively correlated with Al_2O_3 but with lower correlation coefficients (r: 0.69, 0.70, 0.72, respectively). The significant correlation between TiO_2 and Ba (r: 0.88) reveals that the latter is hosted not only in feldspar but also in biotite. Y and Nb are positively correlated with TiO_2 (r: 0.62, 0.94, respectively), whereas Zr and Hf are strongly correlated within themselves but not with TiO_2. Zr content is strongly variable within the interval 206-488 ppm (average: 310 ppm) with seven samples out of ten in the range 206-280 ppm and the remaining three samples (L214, L218, L222) with 417 < Zr < 488ppm. The Zr/Hf ratio between 36 and 43 is quite similar to the average values found in zircons from crustal rocks (Murali *et alii*, 1983; Wang *et alii*, 2010).

The chondrite-normalized REE pattern (according to Sun & McDonough, 1989) of the Lula paragneiss (Fig. 4b) shows significant LREE enrichment (La_N/Sm_N: 3.0-4.3; La_N/Yb_N: 5.2-11.9), with steep slope (sample/chondrite ratios ranging 10-30 for Eu to 70-200 for La), negative Eu anomaly (Eu/Eu* 0.58-0.88) and flat HREE pattern (Gd_N/Yb_N: 1.2-2.0) with sample/chondrite ratio between 7 and 20. Although two paragneiss samples (L216, L218) show relatively lower HREE content, the REE patterns of the paragneiss are comparable and partially overlap with those of the Lula metasandstones reported by Costamagna *et alii* (2012, greyish area in Fig. 4b).

ZIRCON AGE AND CHEMISTRY

All the analyzed zircons belong to a single paragneiss sample (L214). Zircon chemistry and zircon U–Pb geochronological results for paragneiss sample L214 are given in Table S1, whereas CL images of the analysed zircon crystals are shown in Fig. 5. Most crystals show slightly rounded corners and smoothed edges as it is common in sedimentary and metasedimentary rocks. The variable relative development of the two prisms, suggests a wide range of crystallization temperatures, whereas the simultaneous presence of both the {101} and the {211} bipyramids excludes both alkaline and strongly peraluminous rocks among the last sources (Pupin, 1980). CL images reveal multiple magmatic growth stages in most crystals, some of which also contain inherited cores (Fig. 5).

The chemical composition of the crystals varies over a relatively wide range (Table S1) and the obtained ages cover a very large time span (Fig. 6). This is a clear indication that the detrital zircon population of the paragneiss has a complex history of inheritance and recycling. The Y_2O_3 vs HfO_2 diagram, which after Pupin (2000) is indicative of the different magmatic sources, is reported in Fig. 7a-g separately for the different age groups.

Forty-one analyses were performed on 32 crystals and 27 U-Pb data resulted concordant (Table S2). The oldest datum (3151 ± 97 Ma) was obtained on the relic core of crystal A87. Slightly younger discordant ages were found on both the relic core and the magmatic stage of crystal A73. Both grains are characterized (Fig. 7a) by the lack of Y_2O_3, with HfO_2 between 1.30 and 2.40 %, suggesting provenance from a mainly crustal source (calcalkaline or aluminous / peraluminous granites), as also supported by Zr / Hf ratios between 45 and 24 (average 35) (Wang *et alii*, 2010).

Proterozoic ages (1932 ± 11 Ma and 1845 ± 10Ma) were recorded by the main magmatic domain of crystals B36 and B8, respectively. Discordant ages in the same time span were found in crystals B5, A6 and A71. Crystals B8 and B5 show very low Y_2O_3 contents and HfO_2 < 1.1 % (Fig. 7b), suggesting, together with average Zr / Hf ratios around 60, crystallization in relatively dry and hot magmas (Wang *et alii*, 2010). Both grains show only a thin rim slightly enriched in Hf. The other crystals show wider variations, with HfO_2 always > 1.2 %, Y_2O_3 < 0.3 %, Zr / Hf average ratios between 45 and 31, compatible with zircons from calcalkaline (B36) and aluminous granitoids (A6, A71).

The cores of B36 and B8 (as well as the rounded core of A9, not dated but obviously older than 1071 ± 50 Ma) stand out for their relative enrichment in Y_2O_3. The occurrence of a younger rim (801 ± 10 Ma) on B36 (Fig. 7e) suggests recycling of some of these Proterozoic zircons during the genesis of younger magmas.

Other recycled components (1259 ± 51 and 1203 ± 52 Ma) are documented by the cores of crystals A10 and A83, both relatively enriched in Y and Hf (Fig. 7c), as it is often observed in zircons from alkaline subsolvus granites (Pupin, 2000), and with Zr / Hf ratios in the range 42 - 23. A similar composition, also in terms of Zr / Hf ratios (38-36), is shown by a zoned domain of crystal A22, which grows on an irregularly shaped core with different composition and slightly older discordant age (about 1459-1340 Ma). In A83 the fractured core is sealed by

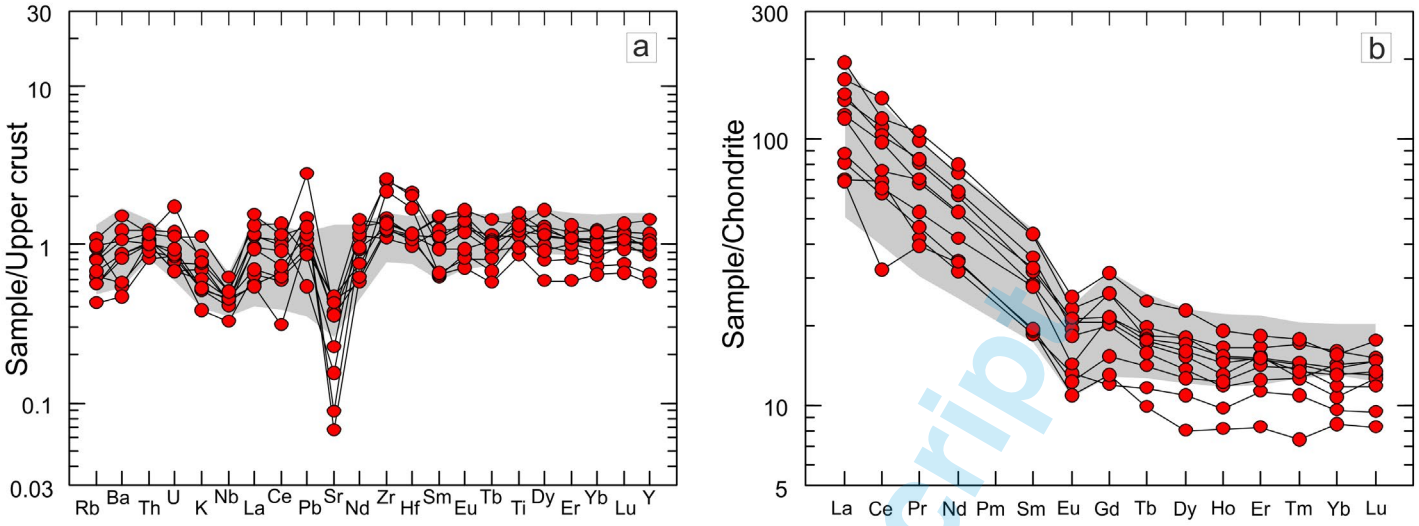

Fig. 4 - Multielement diagrams of Lula paragneiss: a) trace element diagram normalized to the upper crust according to Rudnick & Fountain (1995); b) REE pattern normalized to chondrite according to Sun & McDonough (1989). The grey area shows the compositional range of the Lula metasandstones from Costamagna *et alii* (2012).

a thin zone extremely enriched in Hf, typical of growth from hydrous residual melts (Pérez-Soba *et alii*, 2007), in turn enveloped by a zoned magmatic domain (plotted in Fig. 7f) which gives a much younger concordant age (707 ± 32 Ma). In A10 the core is followed by two growth stages; the first one, zoned and with an irregular outline, for its composition fits well with the age group around 1000 Ma (Fig. 7d), whereas the last one ("rim") is more similar to younger phases (Fig. 7e).

Concordant ages between about 1000 and 1100 Ma were recorded on the main magmatic domain of crystals A1, A9, A84, B38, A3 (two stages with an age difference of 25 Ma), and on the most external zoned domain ("rim") of A22. Their compositional range (Fig. 7d) is compatible with crystallization in a calcalkaline or K-calcalkaline environment of intermediate to acidic composition (diorites to granites), with a general trend of increasing Hf from the inner toward the outer zones; a similar compositional variation is shown by crystal A34, giving a discordant age in the same range, and by the main magmatic domain of crystal A10, not dated but obviously younger than 1200 Ma. The partly corroded core of A111 and the more external magmatic phase of B6, with more or less discordant ages across 1000 – 1100 Ma, plot in the less evolved portion of the distribution field, with HfO_2 between 0.85 and 1.17, Y_2O_3 = 0 and Zr / Hf in the range 68-50. The cores of crystals B32 and B4, not dated but older than about 650 m.y, have been tentatively ascribed to this age group. The obtained results indicate that zircons from magmatic rocks aged around 1100 – 1000 Ma are amongst the main components of the sample population, but some of them were also recycled as crustal materials in the genesis of younger magmas.

Concordant ages between about 950 and 800 Ma were obtained on the main magmatic domains of crystals A86 and A13 (in the latter accompanied by a slightly younger discordant age on a more external area) and on magmatic domains growing on a slightly older (B38) or a much older core (B36). This suggests that the magmas of that age incorporated an already heterogeneous crustal component. The HfO_2 contents always > 1.2 % with very low or absent Y_2O_3 (Fig. 7e) and the progressive enrichment in Hf within the crystals (Zr / Hf decreasing from 47 to 23) are compatible with calcalkaline or K-calcalkaline granodiorites - granites (Pérez-Soba *et alii*, 2007; Wang *et alii*, 2010). The main magmatic phase of crystal A111, which should be younger than about 1000 Ma, fits well within this group. As told before, the Hf-enriched rim of crystal A10 could also belong to this group. On the contrary, the relic core of crystal B7, in spite of its similar concordant age, is completely different (Fig. 7e) for its very low HfO_2 content (Zr / Hf > 70), indicative of a greater mantle contribution in the magma genesis.

Two concordant ages of 757 ± 33 Ma (A17) and 707 ± 32 Ma (A83) represent the youngest ones found in the less magnetic fraction. The older age corresponds to the main magmatic phase of the grain, showing a calcalkaline or K-calcalkaline affinity with limited HfO_2 enrichment (Fig.7f). The younger age represents the external area of A83, showing regular magmatic zoning and similar in composition to the most enriched portion of grain A17.

Concordant ages of 638 ± 12, 648 ± 28, 665 ± 10 Ma are found on crystals B4 (zoned domain corroding and penetrating the core), B32 (external area) and B7 (last growth stage), respectively. The chemical composition in the Y_2O_3 vs HfO_2 diagram (Fig. 7f) is compatible with calcalkaline or K-calcalkaline intermediate rocks (Zr / Hf in the range 65-39). Only the last stage of B4, which morphologically seems to be not much younger, is distinctly enriched in Hf (average Zr / Hf = 24) as in evolved granitic rocks (Pérez-Soba *et alii*, 2007).

The sedimentation age of the protolith is constrained by the youngest age (465 ± 8 Ma), which was found on one crystal of the more magnetic fraction (B10). Two other grains of the same fraction give slightly older ages: B1 (557 ± 10 and 568 ± 8 Ma) and B2 (570 ± 11 and 570 ± 25 Ma). The chemical composition of the latter two crystals (Fig. 7g) is characterized by extremely low or

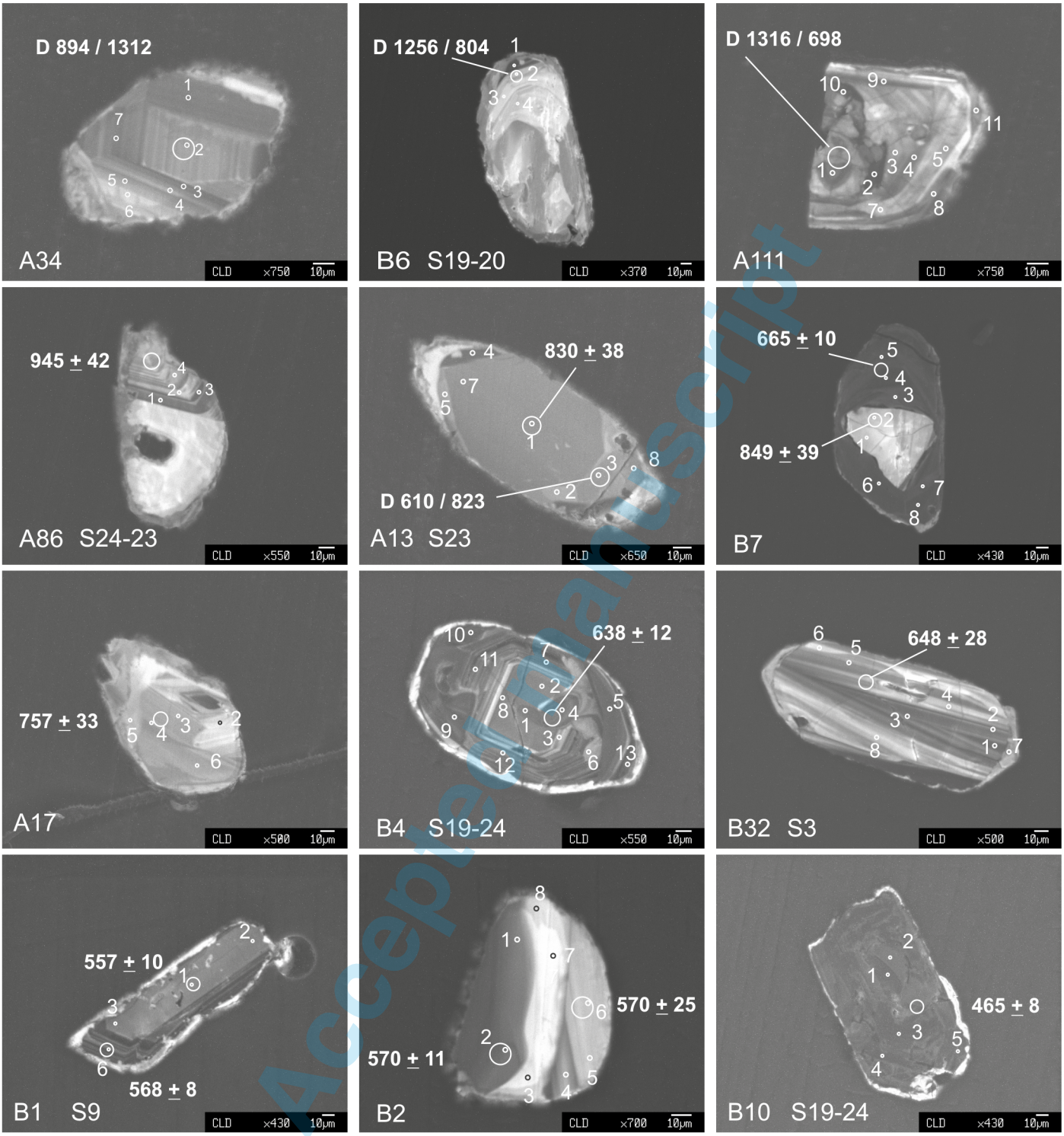

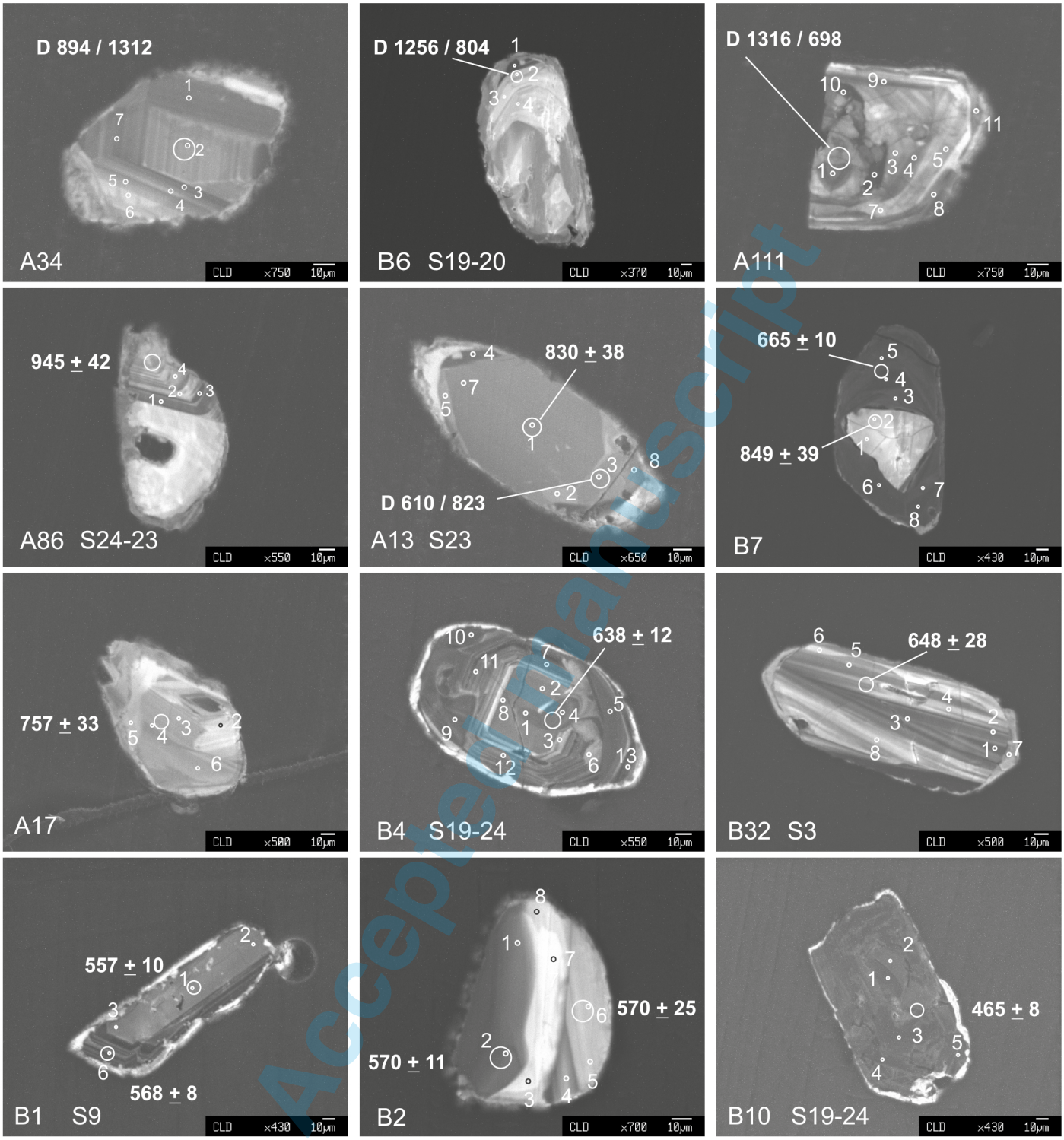

Fig. 5 - Cathodoluminescence images of the analysed zircons from sample L214. Small circles: sites of EMP analyses; large circles: sites of LA analyses with the obtained age (labelled with "D" when discordant). The external typology of each crystal is also indicated.

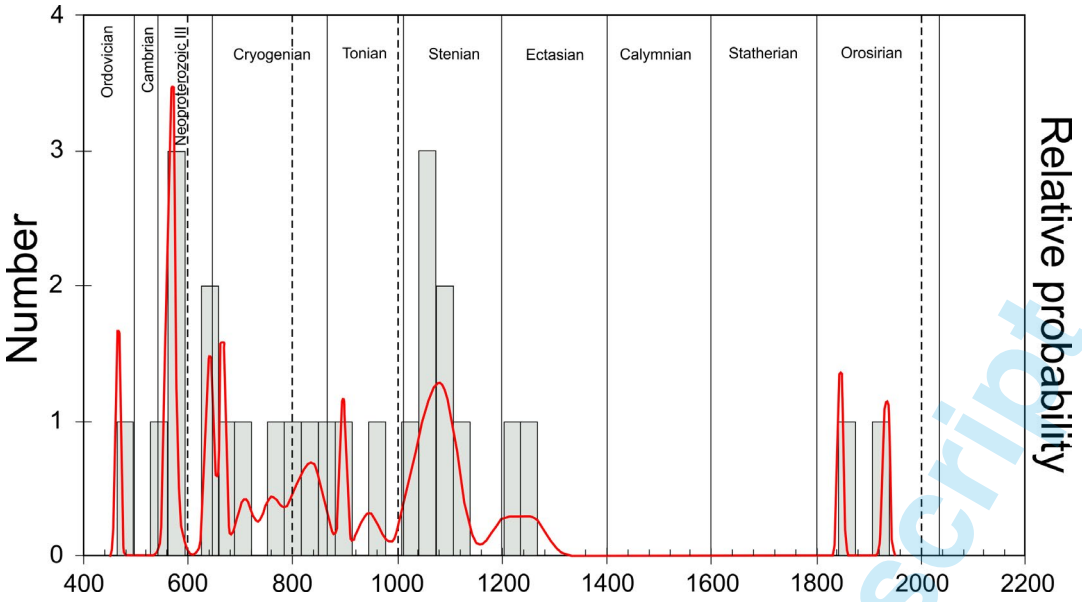

Fig. 6 - Probability density plots for the U–Pb concordant ages obtained for Lula paragneiss sample L214.

absent Y_2O_3, with HfO_2 always below 1.35. Such values are indicative of a mixed mantle – crustal origin (Pupin, 2000), as also suggested by the Zr / Hf ratios between 72 and 43 (Wang *et alii*, 2010). The youngest crystal, B10, is slightly enriched in both elements (Fig. 7g); it also stands out for the highest UO_2 contents observed in the data set (up to 0.65 %).

As a whole, it seems that the oldest ages correspond to the most enriched zircon compositions, as can be found in granitoid rocks of mainly crustal origin. With decreasing ages, the chemical composition is progressively poorer in both Hf and Y and becomes more characteristic of calcalkaline and K-calcalkaline rocks with increasing mantle contribution in their genesis.

DISCUSSION

Source rock of Lula paragneiss and tectonic setting

The Chemical Index of Alteration (CIA) values of the studied samples are in the 59-76 range, with six samples out of ten characterized by CIA< 70 (low degree of alteration of source rocks) and four samples with CIA>70 (larger amounts of clay fraction and/or increasing weathering intensity of the source). The progressive increase of alteration (i.e. weathering trend) from the samples with the lowest CIA values to those with the highest ones can be followed in the A-CN-K triangular diagram after Nesbitt & Young (1982) shown in Fig. 8. The less weathered samples plot close to the A-CN side, overlapping with the Lula metasandstones of Costamagna *et alii* (2012), whereas the most weathered samples (L218, L222) are close to the opposite A-K side.

A comparison of the REE pattern of the paragneiss samples with those observed for Sardinia metavolcanics and for some reference samples as North American Shale Composite (NASC) and Post Archaean Australian Shales (PAAS) provides some valuable clues on their source rock and provenance.

The REE pattern of the six paragneiss samples (L18-19, L66, L214-215, L222) characterized by the highest REE content (128ppm <ΣREE<195ppm) is almost coincident with that of NASC and PAAS. The four samples with the lowest REE abundance (72<ΣREE<107ppm) are significantly depleted in LREE and slightly depleted in HREE as compared to the REE pattern of NASC and PAAS.

The paragneiss samples display, on average, lower ΣREE and slightly less pronounced negative Eu anomalies than the Sardinian Ordovician metavolcanics from Sarcidano, Sarrabus and Gerrei published by Giacomini *et alii* (2006) and Gaggero *et alii* (2012). However, their significant LREE enrichment, the significant negative Eu-anomalies with Eu/Eu* between ~ 0.6-0.9 and the flat HREE pattern indicate a derivation from an old upper continental crust mainly composed of felsic rocks. In the Hf vs. La/Th diagram (Floyd & Leveridge, 1987), the majority of samples plot within, or very near to, the acidic arc source field, with only three samples, characterized by Hf > 9ppm, shifted towards the increasing old sediment component and passive margin field (Fig. 9a). The La/Sc vs. Co/Th diagram shown in Fig. 9b confirms the felsic provenance with the clustering of the studied samples around and between the two points representative of granites and felsic volcanic rocks. Furthermore, the diagram of Fig. 9c shows that all the studied samples match the Zr/Sc, Th/Sc ratios tipycal of the upper crust. On the Eu/Eu* vs. Gd_N/Yb_N (McLennan & Taylor, 1991) diagrams (Fig. 9d), the studied samples show affinity with post-Archean rocks. In the latter diagram, they plot very close to the Upper Continental Crust (UCC) and partially overlap with the metasandstones of the Lula area reported by Costamagna *et alii* (2012).

Some implications for the tectonic setting of the studied rocks can be obtained from the discriminant diagrams that are based on major and some trace elements.

The Th-Co-Zr/10 diagram (Bhatia & Crook, 1986; Fig. 10a) suggests a continental margin provenance with most of the paragneiss samples (seven out of ten) in the B field (continental island arc) and the remaining three (L214, L218, L222), characterized by higher Zr, shifted

towards the Zr/10 apex, at the boundary of the D field (passive continental margin). Similar results are given by the Th-Sc-Zr/10 diagram in which most of the samples are clustered in the B field (not shown). In the triangular diagram La-Th-Sc (Fig. 10b) five samples plot in the B field, three samples plot at the boundary between B and C+D fields and two samples plot in the C, D field. These results confirm that the sedimentary materials were supplied by dismantling of an older active continental margin or island arc.

The obtained ages of the detrital zircons in the paragneiss are consistent with a pre-Variscan Middle Ordovician sedimentary sequence. This seems to contradict the suggestion that the paragneiss are a lower Paleozoic basement with a pre-Variscan deformation and metamorphism (Helbing & Tiepolo, 2005). Moreover, the new U/Pb zircon ages also indicate that this metasedimentary sequence could not be the host rock of the protolith of the Lodè-Mamone orthogneiss. Thus, the Lula paragneiss likely represents a record of an early Paleozoic sedimentary basin which collected sediments from nearby emerged lands consisting of pre-Paleozoic sequences and Early Paleozoic volcanic arc. The U/Pb zircon age of 474 ± 13 Ma reported for the metavolcanics intercalated with metasediments (Helbing & Tiepolo, 2005) reinforce the suggestion that the low to medium metamorphic grade sequence exposed in northeast Sardina correspond to an Early Paleozoic sedimentary basin. This attribution fit well with the suggestion that (i) this sequence experienced a unique Variscan orogenic cycle (Carmignani *et alii*, 1994; Franceschelli *et alii*, 2005) and (ii) a Precambrian basement is absent in the Paleozoic sequence of Sardinian Variscan belt as suggested by Cruciani *et alii* (2019a). Therefore, two different hypotheses can be made regarding the Ordovician tectonic setting: if we consider the Ordovician magmatism developed as an Andean-type magmatic arc, the Lula paragneiss and Lodé orthogneiss would correspond to fore-arc basin and deep portion of magmatic arc respectively. Otherwise if we consider the hypothesis of a middle Ordovician magmatic arc in a subduction-accretionary margin, ("early Paleozoic subduction-accretionary complex"; Zurbriggen 2015; Cruciani *et alii*, 2019a), the Lula paragneiss derives from the part of a Middle Ordovician accretionary wedge located along the northern Gondwana margin (Cenerian Belt; Zurbriggen, 2015, Zurbriggen *et alii*, 1997). In this interpretation the Lodé orthogneiss constitutes the deep portion of the magmatic arc itself emplaced within the accretionary wedge, as suggested by Cruciani *et alii* (2019) for the Monte Filau Ortogneiss in SW Varican belt of Sardinia. Regardless of their interpretation the Lodé orthogneiss and Lula paragneiss were deformed under amphibolites facies conditions and stacked in the Variscan nappe pile during the late Carboniferous D_2 phase.

Zircon age comparison with early Paleozoic units of Sardinia and northern Apennines

The ages obtained in the present study on the zircon population of the paragneiss sample L214 are compared with the radiometric age determinations available in literature for similar rocks from Variscan Sardinia and from the Paleozoic Tuscan metamorphic basement (Table 2).

A quartz-arenite of the Cabitza Formation (Iglesiente-Sulcis, Sardinia) gave U-Pb zircon ages in the 500 Ma-2.5Ga range (Pavanetto *et alii*, 2012) with three main peaks at 647 Ma, 850 Ma and 1 Ga. The remaining zircon grains span between 1.8 Ga and 2.7 Ga. In the nearby Bithia Unit, radiometric age constraints from a quartzarenite (Pavanetto, 2011) range between 500 Ma and 3 Ga. Two populations yielded peaks at 660 and 736 Ma and a third, minor population, gives ages between 900 and 1,050 Ma.

TABLE 2

Comparison between radiometric age determinations of the Lula paragneiss with those, available from literature, of metasedimentary rocks from Variscan Sardinia and Tuscan metamorphic basement. The underlined ages represent the sedimentary ages of the formations.

	Per. - Carb.	Ord.	Cambr.	Neo-prot.	Meso-prot.	Paleo-Prot.	Archean
Lula paragneiss		465	557, 568, 570	638, 648, 665, 707, 757, 800 - 900	1000-1100, 1203, 1259	1845, 1932	3151
Cabitza			550	647 - 850	1000-1200		
Bithia			500	660, 736	900-1050		
Sarrabus		441			1000	1900	
Lower Phyllite			500	640			2540 - 2799
Upper Phyllite			529	540 - 750	1055	1763 - 1877	2530 - 2600
Calamita Schist		461	540	581 - 1005	1055 -		2598
Buti Phyllite			540	615, 755, 865		1825 - 1930	2425 - 2590
San Lorenzo schist	260 - 355	435 - 470	520	615 - 690	1010		
Verrucano	265 - 320	420 - 485	500	760			
Farma Fm.	345 - 370	470 - 480		640		1918 - 2115	2985

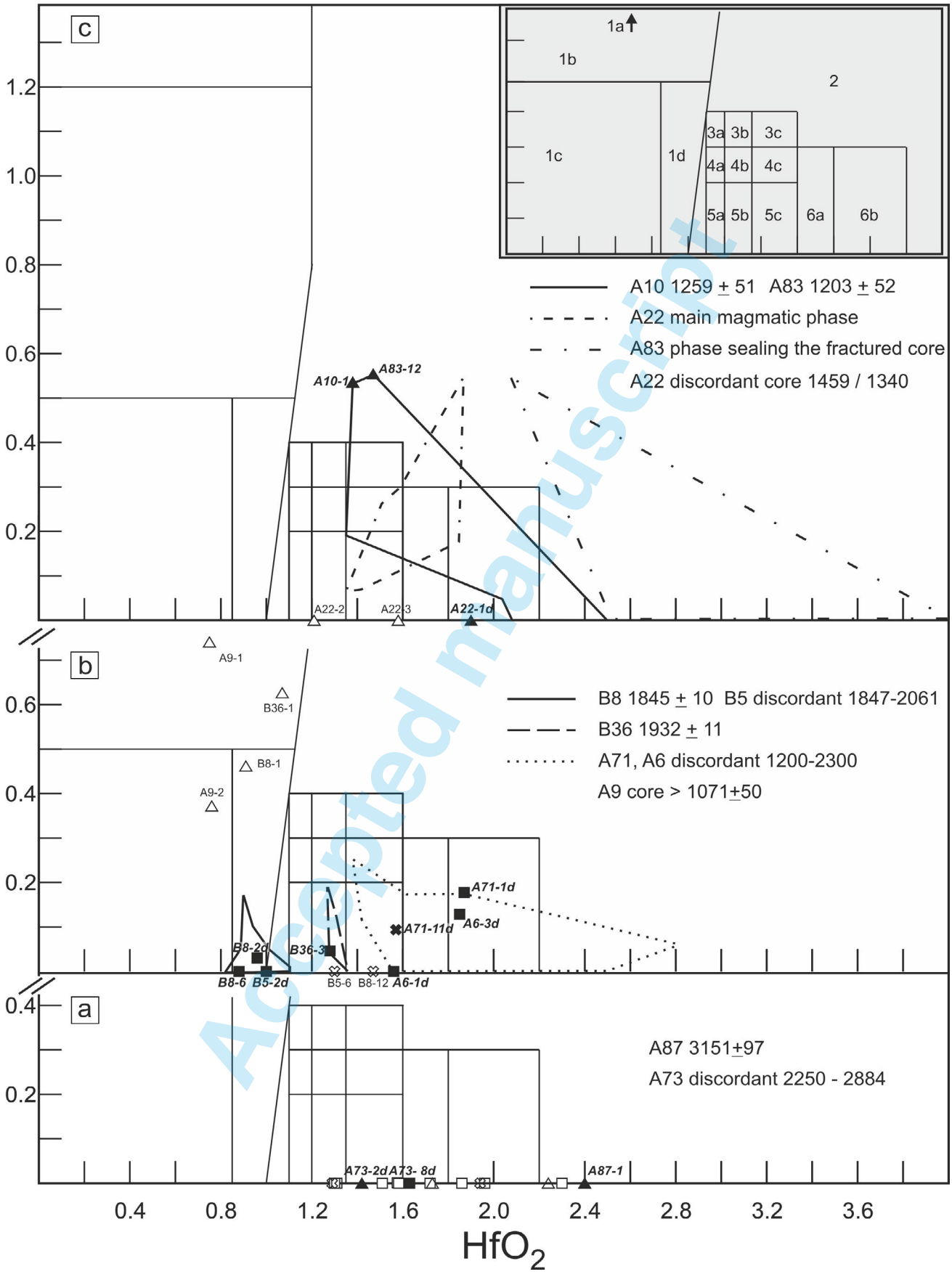

Fig. 7 - Distribution of the analyzed zircons, ordered in a), b), c), d), e), f), g) according to zircon age groups, in the Y_2O_3 vs. HfO_2 diagram from Pupin (2000). The points corresponding to the dated domains are individually plotted and those nearest to the LA dated spots are evidenced with black symbols (with "d" indicating a discordant age); the other analyses are plotted as distribution areas.

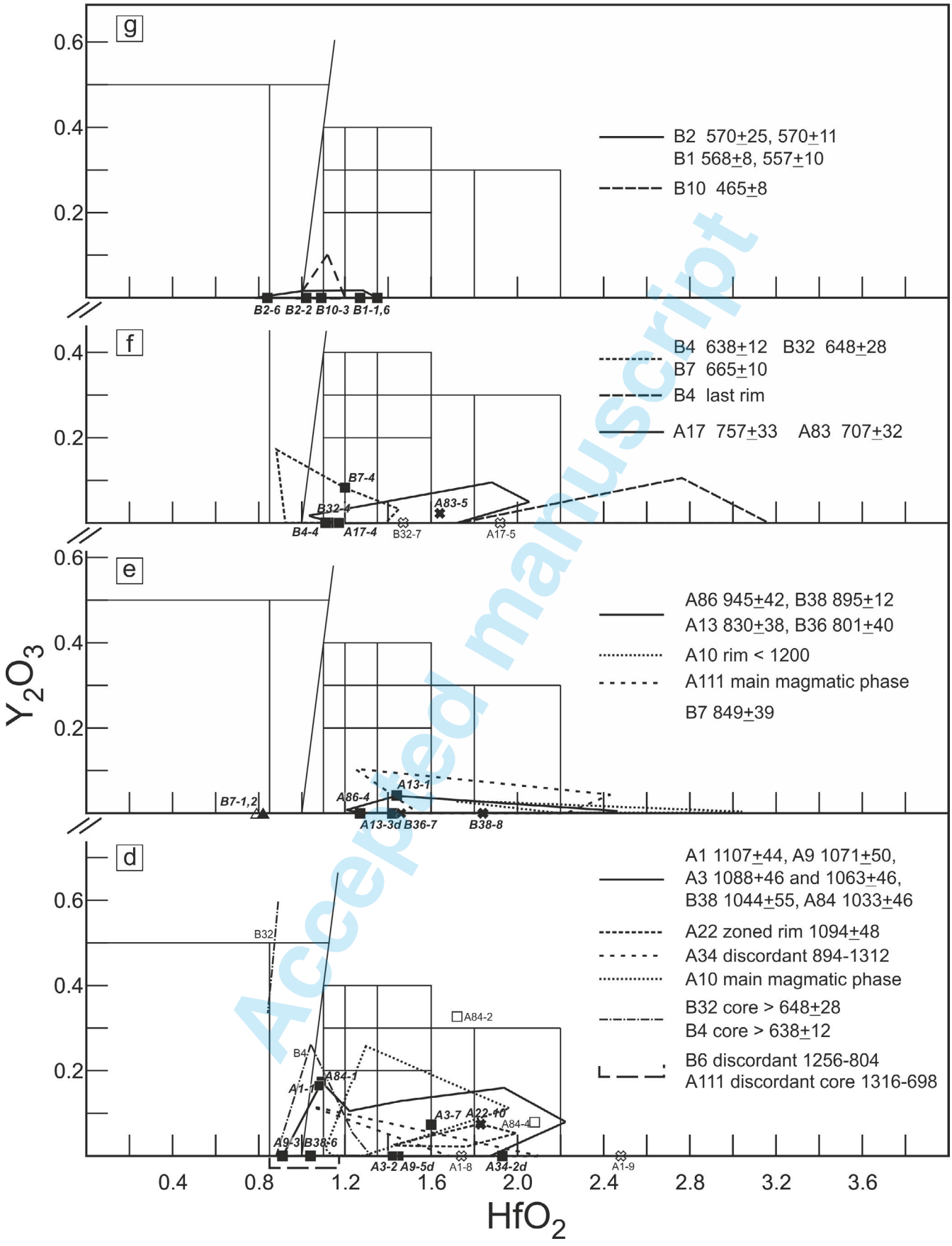

Symbols: triangle = core; square = magmatic phase; cross = rim. Main distribution fields (greyish upper right corner) simplified after Pupin (2000): 1 = mafic rocks of dominant mantle origin; 2 and 3a, b, = anorogenic alkaline subsolvus granites / rhyolites; 3c, 4c, 5c and 6a, b = peraluminous porphyritic granites and leucogranites; 4 and 5: calcalkaline and K-calcalkaline rocks (mafic to acidic from a to c).

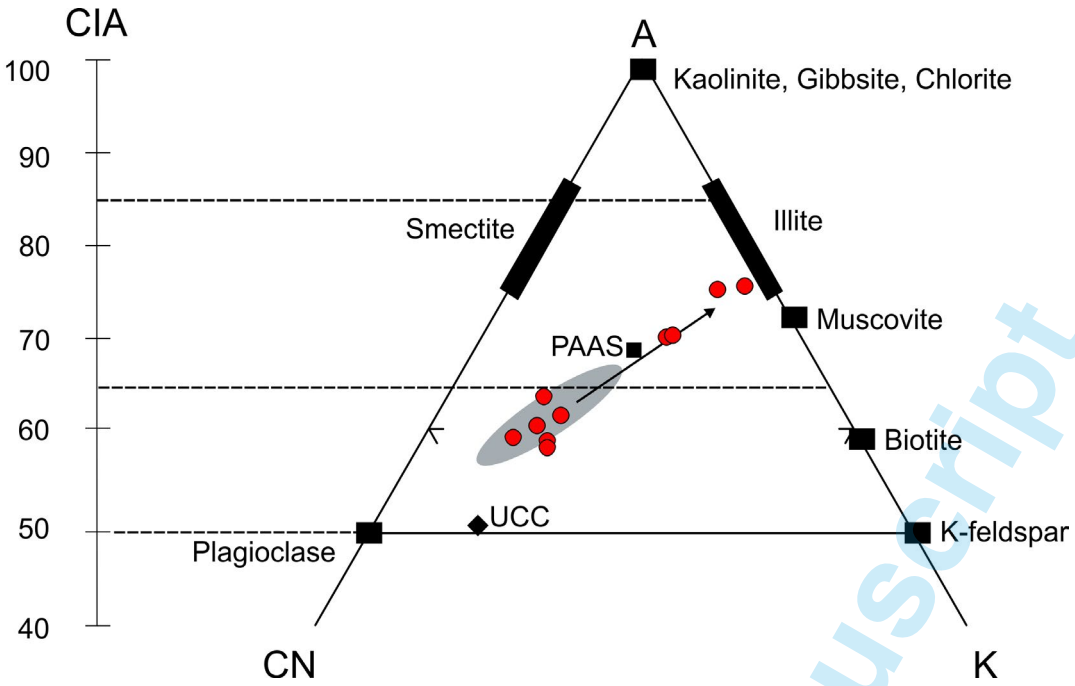

Fig. 8 - A-CN-K triangular diagram after Nesbitt & Young (1982) for the Lula paragneiss. The grey area shows the compositional range of the Lula metasandstones from Costamagna *et alii* (2012). The arrow shows the weathering trend from samples with the lowest CIA values to those with the highest ones. UCC: average upper continental crust from Rudnick & Gao (2003); PAAS: Post Archean Australian Shales from Taylor & McLennan (1985).

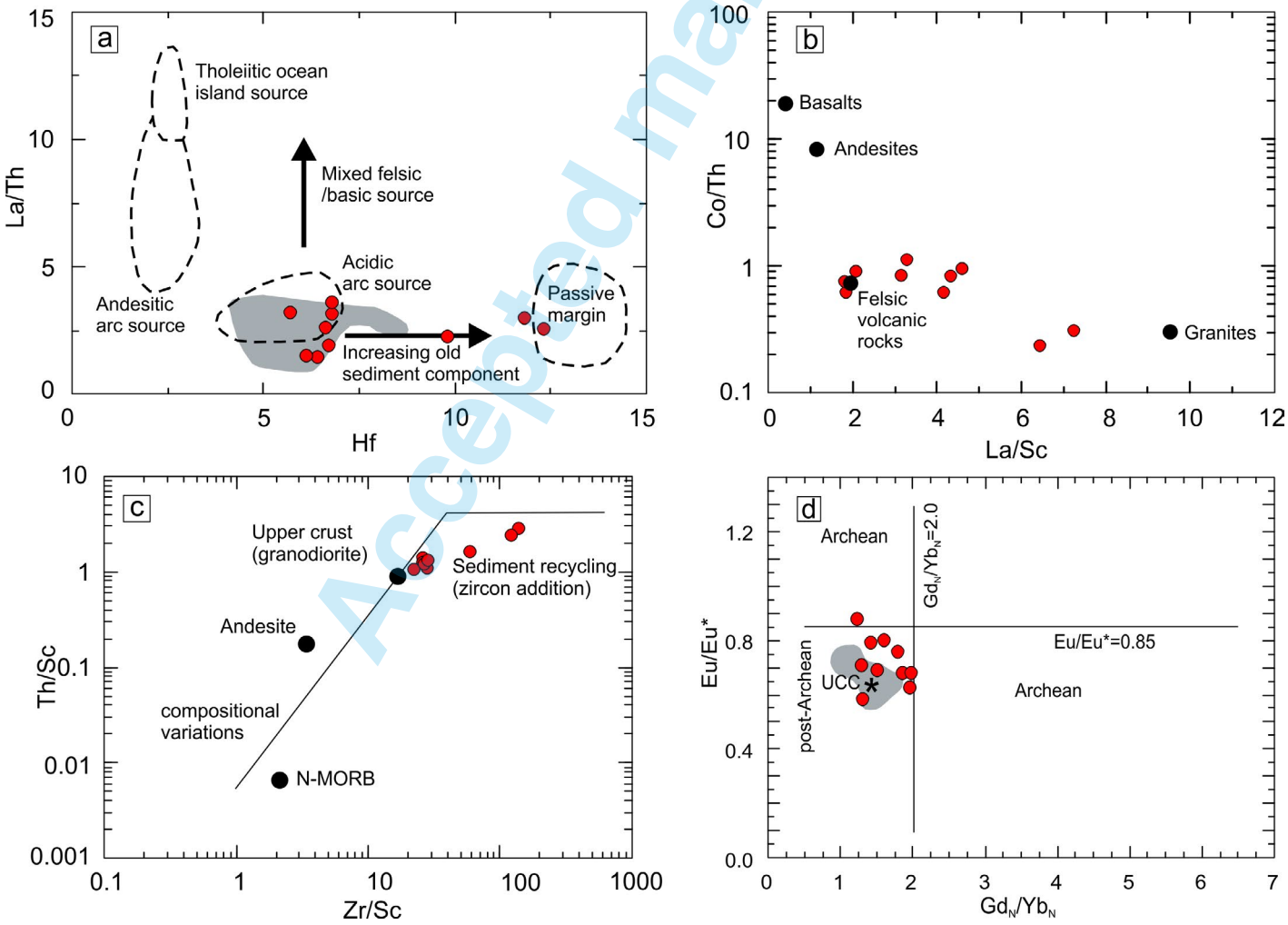

Fig. 9 - (a) La/Th vs. Hf, (b) Co/Th vs. La/Sc, (c) Th/Sc vs. Zr/Sc and (d) Eu/Eu* vs. Gd_N/Yb_N diagrams for the Lula paragneiss. The grey area in (a) and (d) shows the compositional range of the Lula metasandstones from Costamagna *et alii* (2012). UCC: Upper Continental Crust.

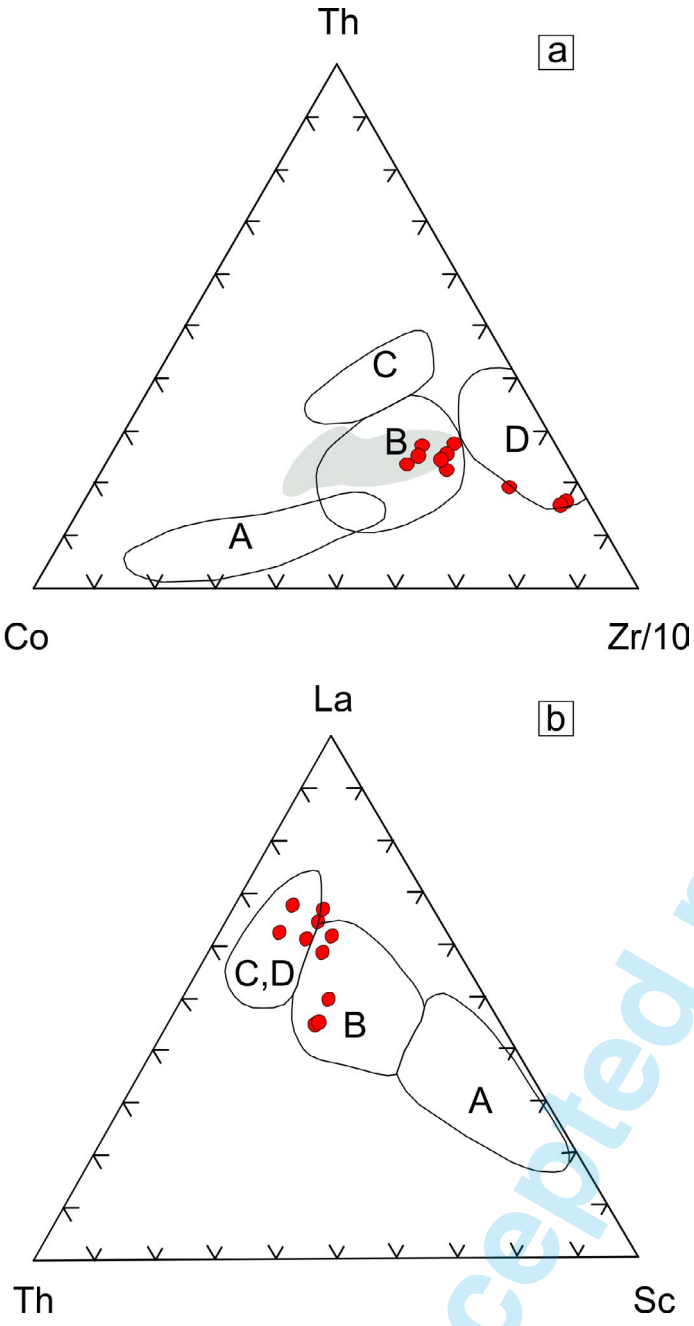

Fig. 10 - a) Th-Co-Zr/10 diagram after Bhatia & Crook (1986), and b) La-Th-Sc diagram for the Lula paragneiss. A: ocean island arc; B: continental island arc; C: active continental margin; D: passive continental margin. In a) the grey area shows the compositional range of the Lula metasandstones from Costamagna *et alii* (2012).

Other scattered zircon grains range between 1,768 Ma and 2,900 Ma. A quartzarenite from the Pta Serpeddi Fm (Sarrabus Unit) yield U-Pb ages within 400 Ma - 2 Ga with a main 360Ma - 750Ma cluster of ages and a main peak at 441 Ma.

In the Tuscan basement, Paoli *et alii* (2017) obtained U–Pb detrital zircon ages from metasedimentary units, for which a summary is given below. A sample from the Lower Quartzite-Phyllite of the Apuan Alps shows ages in the range 1030 - 500 Ma with a main peak at ca. 640 Ma and minor ones at 790 and 915 Ma. In a sample of the Upper Quartzites-Phyllites the major populations are 1055–850 Ma and 750–540 Ma. A Neoarchean population 2600–2530 Ma and a Paleoproterozoic one of ca. 1980–1865 Ma also occur. In the Monti Pisani Buti Quartzites–Phyllites, most of the zircons show continuous age distribution with main peaks at ca. 615, 755 and 865Ma. A sandstone from the San Lorenzo Schists of Monti Pisani shows zircon ages younger than ca. 1010 Ma, with clusters at ca. 355–260 Ma, 470–435 Ma and 615–520 Ma. In the Verrucano sequence the main zircon populations are 320–265 Ma, 485–420 Ma, and 760–500 Ma. In a meta-turbidite sample from the Farma Formation (Monticiano-Roccastrada), a continuum of ages is observed from ca. 640 to 445 Ma with a main peak at ca. 480–470 Ma.

The Calamita Schist in the Elba island reveals age distribution from Proterozoic to early Paleozoic ages (early Cambrian; Sirevag *et alii,* 2016), with the youngest igneous zircons dated at middle-late Ordovician (Musumeci *et alii*, 2011).

Considering the wide range of ages recorded by the detrital zircons in the above mentioned lithological units, a long history emerges with several episodes of both magmatic activity and erosion-sedimentation cycles along the northern margin of Gondwana (Williams *et alii,* 2012). The comparison with the other metasedimentary formations of the early Paleozoic basement in Sardinia and Tuscany (Table 2), outlines a similarity of records of the Lula paragneiss with the Cabitza and Bithia formations as regards the contribution of zircons of Cambrian, Neo and Mesoproterozoic age. Furthermore, a similarity also occurs with the upper Quartzites-Phyllites formation and the Buti Quartzites–Phyllites (Tuscan Paleozoic basement) for the Cambrian and Neoproterozoic ages, but not for the Greenvillian ones.

It could be hypothesized that they represent different portions, probably contiguous or in lateral continuity, of the same continental margin, with a similar and/or common detrital contribution at least by the Neoproterozoic (Panafrican - Cryogenian) and partly also for the Mesoproterozoic (Greenvillian). According to the suggestion of Avigad *et alii* (2012) for the Cabitza formation, on the basis of similar content of Cambrian and Neoproterozoic detrital zircons, a derivation of the Lula paragneiss from Pan-African terranes along the northern Gondwana margin can be proposed.

Moreover, the occurrence of Greenvillian zircons in metasediments of the SW Sardinia early Paleozoic basement (i.e. Cabitza and Bithia formations) and the Lula paragneiss could indicate a contribution from the Sahara craton and/or the Arabian-Numidian shield (Fig. 11) along the northeastern margin of Gondwana (Avigad *et alii*, 2012).

Similar deductions were also proposed for the Calabria–Peloritani Terrane of Southern Italy, where some pre-Cambrian sediments derive from East and West African sources and the Ordovician sediments reflect erosion of Pan-African orogen and local input from Grenvillian terrains (Fornelli *et alii,* 2016).

CONCLUSIONS

The geochemical data and U–Pb analyses of zircon of some samples of Lula paragneiss from tectonic domains in the axial zone of Variscan belt in northern Sardinia,

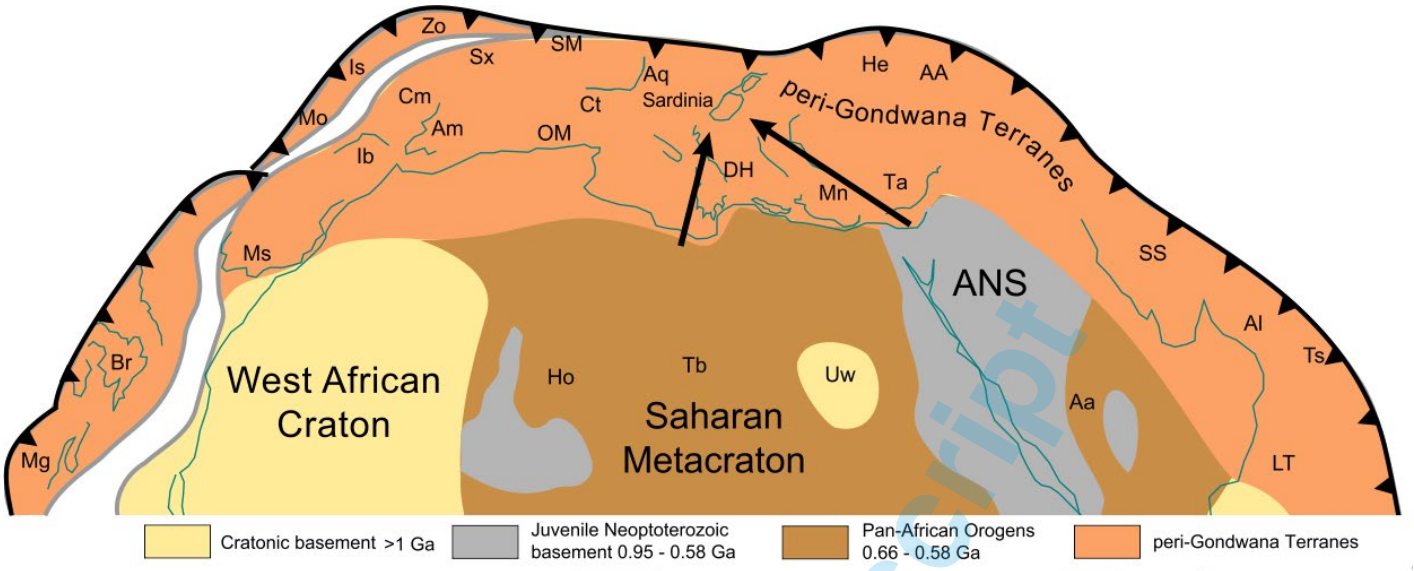

Fig. 11 - Cambrian reconstruction of Gondwana showing the main geotectonic units and the location of the study area on the North Gondwana edge (modified from Avigad *et alii*, 2017, Abbo *et alii*, 2018). Peri-Gondwana terranes after Stampfli *et alii* (2002). Aa – Afif, AA – Austro-Alpine, Al – Alborz, Am– Armorica, ANS – Arabian–Nubian Shield, Aq – Aquitaine, Br – Britannia, Cm – Cadomia, Ct – Cantabria, DH – Dinarides-Helenides, He – Helvetic, Ho – Hoggar, Ib – allochthons from northwestern Iberia, Is – Istanbul zone, LT – Lut-Tabas, Mg – Meguma, Mn – Menderes, Mo – Moldanubian, Ms – Meseta, OM – Ossa-Morena., SM – Serbo-Macedonian, Sr – Sardinia, SS – Sanandaj-Sirjan, Sx – Saxo-Thuringian, Ta – Taurus, Tb – Tibesti, Ts – south Tarim, Uw –Uweinat, Zo – Zonguldak. The arrows show the provenance of detrital zircons in the Sardinia paragneiss.

contribute to the knowledge of peri-Gondwanan evolution from Late-Proterozoic to early Paleozoic times.

The new data provide evidence of the following geological processes:

- The source rocks of the Lula paragneiss derive from an early-Paleozoic sedimentary basin which collected sediments from the nearby pre-Paleozoic sequences and early Paleozoic volcanic arc.
- The deposition age of the sedimentary protolith, similar to the emplacement age of Lodé orthogneiss, indicates that the Lula paragneiss derives from a fore-arc basin in an Ordovician active convergent margin (Andean-type or subduction-accretion margin). This suggestion contradicts previous interpretation of the Lula paragneiss as host rock of the Lodé orthogneiss and highlights the role of Variscan tectonics in the assembly of different blocks deriving from the early-middle Paleozoic margin.
- The REE pattern of the paragneiss, with LREE enrichment, negative Eu-anomaly and flat HREE, suggests a derivation from an old upper continental crust mainly made up of felsic rocks. The sedimentary material was likely supplied from an older active continental margin or island arc.
- The U-Pb ages obtained from detrital zircons of the paragneiss cover a very large time span (3151 + 97 Ma to 465 + 8 Ma), with the oldest ages corresponding to zircon compositions compatible with granitoid rocks of crustal origin, and the younger ones beeing compatible with calcalkaline and K-calcalkaline rocks with increasing mantle contribution in their genesis.
- A derivation of the sedimentary supply from the Sahara craton and/or the Arabian-Numidian shield along the northeastern margin of Gondwana is suggested by the ages of detrital zircons. This fits well with similar proposed derivation of early Paleozoic metasedimentary formations in southern Sardinia and northern Apennine, pointing out a common location of these sedimentary basins along the northern margin of Gondwana at the early Paleozoic times.

Acknowledgements

We are grateful to one anonymous reviewer and to Annamaria Fornelli who helped to improve the original manuscript. Dr. Antonio Langone (C.N.R.-Istituto di Geoscienze e Georisorse, UOS Pavia) is gratefully acknowledged for geochronological analyses and scientific support in the data interpretation. This work beneficiated from Università di Cagliari funds to M. Franceschelli.

REFERENCES

Abbo A., Avigad D. & Gerdes A. (2018) - *The lower crust of the Northern broken edge of Gondwana: evidence for sediment subduction and syn-Variscan anorogenic imprint from zircon U-Pb-Hf in granulite xenoliths*. Gondwana Res., **64**, 84-96.

Avigad D., Gerdes A., Morag N. & Bechstädt T. (2012) - *Coupled U–Pb–Hf of detrital zircons of Cambrian sandstones from Morocco and Sardinia: Implications for provenance and Precambrian crustal evolution of North Africa*. Gondwana Res., **21**, 690-703.

Avigad D., Morag N., Abbo A. & Gerdes A. (2017) - *Detrital rutile U-Pb perspective on the origin of the great Cambro-Ordovician sandstone of North Gondwana and its linkage to orogeny.* Gondwana Res., **51**, 17-29.

Bakkiaraj D., Nagendra R., Nagarajan R. & Armstrong-Altrin J.S. (2010) - *Geochemistry of sandstones from the Upper Cretaceous Sillakkudi Formation, Cauvery Basin, Southern India: implication for provenance*. J. Geol. Soc. India, **76**, 453-467.

Barca S., Carmignani L., Eltrudis A. & Franceschelli M. (1995) - *Origin and evolution of the Permian-Carboniferous basin of Mulargia Lake (South-Central Sardinia, Italy) related to the Late-Hercynian extensional tectonic.* C.R. Acad. Sciences Paris, **321**, IIa, 171-178.

Bhatia M.R. & Crook K.A.W. (1986) - *Trace element characteristics of greywackes and tectonic setting discrimination of sedimentary basin*. Contrib. Mineral. Petrol., **92**, 181–193.

Carmignani L., Carosi R., Di Pisa A., Gattiglio M., Musumeci G., Oggiano G. & Pertusati P.C. (1994) - *The Hercynian Chain in Sardinia (Italy)*. Geodin. Acta, **7**, 31-47.

Carmignani L., Oggiano G., Barca S., Conti P., Salvadori I., Eltrudis A., Funedda A. & Pasci S. (2001) - *Geologia della Sardegna*. Note illustrative della Carta Geologica della Sardegna a scala 1:200.000. Mem. Soc. Geol. It., **60**, 283 pp.

Carosi R., Di Pisa A., Iacopini D., Montomoli C. & Oggiano G. (2004) - *The structural evolution of the Asinara Island (NW Sardinia, Italy)*. Geodin. Acta, **17**(5), 309-329.

Carosi R., Frassi C., Iacopini D. & Montomoli C. (2005) - *Post collisional transpressive tectonics in northern Sardinia (Italy)*. J. Virtual Explorer, **19**, paper 3.

Carosi R., Frassi C. & Montomoli C. (2009) - *Deformation during exhumation of medium- and high-grade metamorphic rocks in the Variscan chain in northern Sardinia (Italy)*. Geol. J., **44**, 280-305.

Carosi R. & Palmeri. R. (2002) - *Orogen-parallel tectonic transport in the Variscan belt of northeastern Sardinia (Italy): implications for the exhumation of medium-pressure metamorphic rocks*. Geol. Mag., **139**(5), 497-511.

Connolly J.A.D., Memmi I., Trommsdorff V., Franceschelli M. & Ricci C.A. (1994) - *Forward Modelling of Ca-silicate microinclusion and fluid evolution in a graphitic metapelite (NE Sardinia)*. Am. Mineral., **79**, 960-972.

Conti P., Carmignani L. & Funedda A. (2001) - *Change of nappe transport direction during the Variscan collisional evolution of central-southern Sardinia (Italy)*. Tectonophysics, **332**, 255-273.

Costamagna L.G., Cruciani G., Franceschelli M. & Puxeddu M. (2012) - *A volcano-sedimentary sequence with albitite layers in the Variscan basement of NE Sardinia: a petrographical and geochemical study.* Per. Mineral., **81**, 179-204.

Costamagna L.G., Elter F.M., Gaggero L. & Mantovani F. (2016) - *Contact metamorphism in middle Ordovician arc rocks (SW Sardinia, Italy): new paleogeographic constraints*. Lithos, **264**, 577–593.

Cruciani G., Dini A., Franceschelli M., Puxeddu M. & Utzeri D. (2010) - *Metabasite from the Variscan belt in NE Sardinia, Italy: within plate OIB-like melts with very high Sr and low Nd isotope ratios.* Eur. J. Mineral., **22**, 509-523.

Cruciani G., Fancello D., Franceschelli M. & Musumeci G. (2019a) - *Geochemistry of the Monte Filau orthogneiss (SW Sardinia, Italy): insight into the geodynamic setting of Ordovician felsic magmatism in the N/NE Gondwana margin*. It. J. Geosci., **138**, 136-152.

Cruciani G., Fancello D., Franceschelli M., Scodina M. & Spano M.E. (2014a) - *Geothermobarometry of Al-silicate-bearing migmatites from the Variscan chain of NE Sardinia, Italy: a P-T pseudosection approach*. Per. Mineral., **83**(1), 19-40.

Cruciani G., Franceschelli M., Foley S.F. & Jacob D.E. (2014b) - *Anatectic amphibole and restitic garnet in some Variscan migmatite from NE Sardinia, Italy: insights into partial melting from mineral trace elements*. Eur. J. Mineral., **26**, 381-395.

Cruciani G., Franceschelli M. & Groppo C. (2011) - *P-T evolution of eclogite-facies metabasite from NE Sardinia, Italy: insights into the prograde evolution of Variscan eclogites*. Lithos, **121**, 135-150.

Cruciani G., Franceschelli M., Groppo C., Oggiano G. & Spano M.E. (2015a) - *Re-equilibration history and P-T path of eclogites from Variscan Sardinia, Italy: a case study from the medium-grade metamorphic complex*. Int. J. Earth Sci., **104**, 797-814.

Cruciani G., Franceschelli M., Langone A., Puxeddu M. & Scodina M. (2015b) - *Nature and age of pre-Variscan eclogite protoliths from the Low- to Medium-Grade Metamorphic Complex of north–central Sardinia (Italy) and comparisons with coeval Sardinian eclogites in the northern Gondwana context*. J. Geol. Soc., **172**, 792-807.

Cruciani G., Franceschelli M., Massonne H.-J., Carosi R. & Montomoli C. (2013b) - *Pressure-temperature and deformational evolution of high-pressure metapelites from Variscan NE Sardinia, Italy.* Lithos, **175-176**, 272-284.

Cruciani G., Franceschelli M., Massonne H.-J., Musumeci G. & Spano M.E. (2016) - *Thermomechanical evolution of the high-grade core in the nappe zone of Variscan Sardinia, Italy: the role of shear deformation and granite emplacement*. J. Metam. Geol., **34**, 321-342.

Cruciani G., Franceschelli M., Musumeci G., Spano M.E. & Tiepolo M. (2013a) - *U-Pb zircon dating and nature of metavolcanics and metarkoses from the Monte Grighini Unit: new insights on Late Ordovician magmatism in the Variscan belt in Sardinia, Italy*. Int. J. Earth Sci., **102**, 2077-2096.

Cruciani G., Franceschelli M., Puxeddu M. & Tiepolo M. (2018) - *Metavolcanics from Capo Malfatano, SW Sardinia, Italy: new insight on the age and nature of Ordovician volcanism in the Variscan foreland zone*. Geol. J., **53**, 1573- 1585.

Cruciani G., Franceschelli M., Scodina M. & Puxeddu M. (2019b) - *Garnet zoning in kyanite-bearing eclogite from Golfo Aranci: new data on the early prograde P-T evolution in NE Sardinia, Italy*. Geol. J., **54**, 190-205.

Cruciani G., Montomoli C., Carosi R., Franceschelli M. & Puxeddu M. (2015c) - *Continental collision from two perspectives: a review of Variscan metamorphism and deformation in northern Sardinia.* Per. Mineral., **84**(3B), 657-699.

Fancello D., Cruciani G., Franceschelli M. & Massonne H.-J. (2018) - *Trondhjemitic leucosomes in paragneisses from NE Sardinia: geochemistry and P-T conditions of melting and crystallization.* Lithos, **304-307**, 501-517.

Fernandez-Suarez J., Gutiérrez-Alonso G., Jenner G.A. & Tubrett M.N. (2000) - *New ideas on the Proterozoic-Early Palaeozoic evolution of NW Iberia: insights from U–Pb detrital zircon ages*. Precambrian Res., **102**, 185–206.

Fornelli A., Micheletti F. & Piccarreta G. (2016) - *Late-Proterozoic to Paleozoic history of the peri-Gondwana Calabria–Peloritani Terrane inferred from a review of zircon chronology.* SpringerPlus, **5**, 212.

Floyd P.A. & Leveridge B.E. (1987) - *Tectonic environment of the Devonian Gramscatho basin, south Cornwall: framework mode and geochemical evidence from turbiditic sandstones*. J. Geol. Soc. London, **144**, 531–542.

Franceschelli M., Memmi I., Pannuti F. & Ricci C.A. (1989) - *Diachronous metamorphic equilibria in the Hercynian basement of northern Sardinia, Italy*. In Daly J.S., Cliff R.A. & Yardley BW.D. (eds.) Evolution of metamorphic belts. Geol. Soc. London, Special Publ., **43**, 371-375.

Franceschelli M., Memmi I. & Ricci C.A. (1982) - *Ca distribution between garnet and plagioclase in pelitic and psammitic schists from the metamorphic basement of north eastern Sardinia.* Contrib. Mineral. Petrol., **80**, 225- 295.

Franceschelli M., Puxeddu M. & Cruciani G. (2005) - *Variscan Metamorphism in Sardinia, Italy: review and discussion*. J. Virtual Explorer, **19**, paper 2.

Franceschelli M., Puxeddu M., Cruciani G. & Utzeri D. (2007) - *Metabasites with eclogite facies relics from Variscides in Sardinia, Italy: a review.* Int. J. Earth Sci., **96**, 795-815.

Gaggero L., Oggiano G., Funedda A. & Buzzi L. (2012) - *Rifting and arc-related early Paleozoic volcanism along the north Gondwana margin: geochemical and geological evidence from Sardinia (Italy)*. J. Geol., **120**, 273-292.

Giacomini F., Bomparola R.M., Ghezzo C. & Guldbransen H. (2006) - *The geodynamic evolution of the Southern European Variscides: constraints from the U/Pb geochronology and geochemistry of the Lower Palaeozoic magmatic-sedimentary sequences of Sardinia (Italy).* Contrib. Mineral. Petrol., **152**, 19–42.

Helbing H., Frisch W. & Bons P.D. (2006) - *South Variscan terrane accretion: Sardinian constraints on the intra-Alpine Variscides.* J. Structural Geol., **28**, 1277-1291.

Helbing H. & Tiepolo M. (2005) - *Age determination of Ordovician magmatism in NE Sardinia and its bearing on Variscan basement evolution*. J. Geol. Soc. London, **162**, 689-700.

Herron M.M. (1988) - *Geochemical classification of terrigenous sands and shales from core or log data.* J. Sedimentary Res., **58**, 820–829.

Iacopini D., Carosi R., Montomoli C. & Passchier C.W. (2008) - *Strain analysis and vorticity of flow in the northern Sardinian Variscan belt: recognition of a partitioned oblique deformation event.* Tectonophysics, **446**, 77–96.

Jackson S.E., Pearson N.J., Griffin W.L. & Belousova E. (2004) - *The application of laser ablation inductively coupled plasma mass spectrometry to in-situ U–Pb zircon geochronology.* Chem. Geol., **211**, 47–69.

Ketchum J.W.F., Jackson S.E., Culshaw N.G. & Barr S.M. (2001) - *Depositional and tectonic setting of the Paleoproterozoic Lower Aillik Group, Makkovik Province, Canada: evolution of a passive*

margin—foredeep sequence based on petrochemistry and U–Pb (TIMS and LAM-ICP-MS) geochronology. Precambrian Res., **105**, 331–356.

Leone F., Hamman W., Laske R., Serpagli E. & Villas E. (1991) - *Lithostratigraphic units and biostratigraphy of the post-sardic Ordovician sequence in south-west Sardinia*. Boll. Soc. Paleo. It., **30**(2), 201–235.

Ludwig K.R. (2000) - *Isoplot: a geochronological toolkit for Microsoft Excel*. Berkeley Geochronology Center. Berkeley, Special Publ., 1a, 1–53.

Massonne H.-J., Cruciani G. & Franceschelli M. (2013) - *Geothermobarometry on anatectic melts - a high-pressure Variscan migmatite from northeast Sardinia*. Int. Geol. Rev., **55**, 1490–1505.

Massonne H.-J., Cruciani G., Franceschelli M. & Musumeci G. (2018) - *Anticlockwise pressure-temperature paths record Variscan upper-plate exhumation: example from micaschists of the Porto Vecchio region, Corsica*. J. Metam. Geol., **36**, 55–77.

McLennan S.M. & Taylor S.R. (1991) - *Sedimentary rocks and crustal evolution: tectonic setting and secular trends.* J. Geol., **99**, l–21.

Murali A.V., Parthasarathy R., Mahadevan T.M. & Sankar Das M. (1983) - *Trace element characteristics, REE patterns and partition coefficients of zircons from different geological environments - a case study on Indian zircons*. Geochim. Cosmochim. Acta, **47**, 2047–2052.

Murphy J.B., Gutiérrez Alonso G., Nance R.D., Fernández-Suárez J., Keppie J.D., Quesada C., Strachan R.A. & Dostal J. (2006) - *Origin of the Rheic Ocean: rifting along a Neoproterozoic suture?* Geology, **34**, 325–328.

Musumeci G., Mazzarini F., Tiepolo M. & Di Vincenzo G. (2011) - *U-Pb and ^{40}Ar-^{39}Ar geochronology of Palaeozoic units in the northern Apennines: determining protolith age and alpine evolution using the Calamita Schist and Ortano Porphyroid.* Geol. J., **46**, 288–310.

Musumeci G., Spano M.E., Cherchi G.P., Franceschelli M., Pertusati P.C. & Cruciani G. (2015) - *Geological Map of the Monte Grighini Variscan Complex (Sardinia, Italy)*. J. Maps, **11**, 287–298.

Nance R., Gutiérrez-Alonso G., Keppie J.D., Linnemann U., Murphy J.B., Quesada C., Strachan R.A. & Woodcock N.H. (2010) - *Evolution of the Rheic Ocean*. Gondwana Res., **17**, 194–222.

Nesbitt H.W. & Young G.M. (1982) - *Early Proterozoic climates and plate motions inferred from major element chemistry of lutites*. Nature, **299**, 715–717.

Oggiano G. & Di Pisa A. (1992) - *Geologia della catena Ercinica in Sardegna - Zona Assiale*. In: Carmignani L., Pertusati P.C., Barca S., Carosi R., Di Pisa A., Gattiglio M., Musumeci G. & Oggiano G. (Eds), Struttura della catena ercinica in Sardegna. Guida all' escursione. Gruppo Informale di Geologia Strutturale, 147-177, Siena.

Oggiano G., Gaggero L., Funedda A., Buzzi L. & Tiepolo M. (2010) - *Multiple early Palaeozoic volcanic events at the northern Gondwana margin: U-Pb age evidence from the Southern Variscan branch (Sardinia, Italy)*. Gondwana Res., **17**, 44-58.

Paoli G., Stokke H.H., Rocchi S., Sirevaag H., Ksienzyk A.K., Jacobs J. & Košler J. (2017) - *Basement provenance revealed by U–Pb detrital zircon ages: a tale of African and European heritage in Tuscany, Italy*. Lithos, **277**, 376-387.

Pavanetto P. (2011) - *Zircon U-Pb and Lu-Hf isotopic data from some peri-Gondwana Variscan terranes (Sardinia-Corsica block and calabropeloritan arc): new insights on the Cenozoic geodynamic evolution of the central Mediterranean basin*. Ph.D. Thesis. Università degli Studi di Cagliari. 187 pp.

Pavanetto P., Funedda A., Northrup C. J., Schmitz M., Crowley J. & Loi A. (2012) - *Structure and U–Pb zircon geochronology in the Variscan foreland of SW Sardinia, Italy*. Geol. J., **47**, 426–445.

Pérez-Soba C., Villaseca C. & Gonzalez Del Tanago J. (2007) – *The composition of zircon in the peraluminous Hercynian granites of the Spanish Central System batholith.* Can. Mineral., **45**, 509-527.

Pillola G.L., Leone F. & Loi A. (1995) - *The Lower Cambrian Nebida Group of Sardinia.* Rend. Seminario Facoltà di Scienze dell'Università di Cagliari, supplemento LXV, 27-62.

Pupin J.P. (1980) - *Zircon and granite petrology*. Contrib. Mineral. Petrol., **73**, 207–220.

Pupin J.P. (2000) - *Granite genesis related to geodynamics from Hf – Y in zircon*. Trans. Royal Soc. Edinburgh: Earth Sci., **91**, 245–256.

Ricci C.A., Carosi R., Di Vincenzo G., Franceschelli M. & Palmeri R. (2004) - *Unravelling the tectonometamorphic evolution of medium-pressure rocks from collision to exhumation of the Variscan basement of NE Sardinia: a review*. Special issue 2. A showcase of the Italian research in metamorphic petrology. Per. Mineral., **73**, 73–83.

Rossi P., Oggiano G. & Cocherie A. (2009) - *A restored section of the "southern Variscan realm" across the Corsica–Sardinia microcontinent*. C.R. Geosci., **341**, 224–238.

Rudnick R.L. & Gao S. (2003) - *Composition of the Continental Crust*. In Heinrich D.H. & Karl K.T. (Eds.), Treatise on Geochemistry, Oxford: Pergamon, 1–64.

Rudnick R.L. & Fountain D.M. (1995) - *Nature and composition of the continental crust: a lower crustal perspective*. Rev. Geophys., **33**(3), 267-309.

Scodina M., Cruciani G., Franceschelli M. & Massonne H.-J. (2019) - *Anticlockwise P-T evolution of amphibolites from NE Sardinia, Italy: geodynamic implications for the tectonic evolution of the Variscan Corsica-Sardinia block*. Lithos, **324-325**, 763-775.

Sirevaag H., Jacobs J., Ksienzyk A.K., Rocchi S., Paoli G., Jørgensen H. & Košler J. (2016) - *From Gondwana to Europe: The journey of Elba Island (Italy) as recorded by U–Pb detrital zircon ages of Paleozoic metasedimentary rocks*. Gondwana Res., **38**, 273–288.

Stampfli G.M., von Raumer J.F. & Borel G.D. (2002) - *Paleozoic Evolution of Pre-Variscan Terranes: from Gondwana to the Variscan collision*. Geol. Soc. Am. Special Paper, **364**, 263–280.

Sun S.S. & McDonough W.F. (1989) - *Chemical and isotopic systematics of oceanic basalts: implications for mantle composition and processes*. In: Saunders A.D. & Norry M.J. (eds) Magmatism in the Ocean Basins. Geol. Soc. London Special Publ., **42**, 313–345.

Taylor S.R. & McLennan S.M. (1985) - *The Continental Crust: Its Composition and Evolution*. Blackwell, Oxford, 312 pp.

Tiepolo M. (2003) - *In situ Pb geochronology of zircon with laser ablation inductively coupled plasma-sector field mass spectrometry*. Chem. Geol., **199**,159–177.

Trombetta A., Cirrincione R., Corfu F., Mazzoleni P. & Pezzino A. (2004) - *Mid-Ordovician U-Pb ages of porphyroids in the Peloritan Mountains (NE Sicily): paleogeographic implications for the evolution of the Alboran microplate.* J. Geol. Soc. London, **161**, 265-276.

van Achterbergh E., Ryan C.G., Jackson S.E. & Griffin W.L. (2001) - *Data reduction software for LA-ICP-MS*. In: Sylvester P. (ed.) Laser Ablation-ICPMS in the Earth Science, Mineralogical Association of Canada: St. John's Newfoundland, **29**, 239–243.

Wang X., Griffin W.L. & Chen J. (2010) - *Hf contents and Zr / Hf ratios in granitic zircons*. Geochem. J., **44**, 65–72.

Wiedenbeck M., Allé P., Corfu F., Griffin W.L., Meier M., Oberli F., von Quadt A., Roddick J.C. & Spiegel W. (1995) - *Three natural zircon standards for U–Th–Pb, Lu–Hf, trace element and REE analyses*. Geostandards Newsl., **19**, 1–23.

Williams I.S., Fiannacca P., Cirrincione R. & Pezzino A. (2012) - *Peri-Gondwanan origin and early geodynamic history of NE Sicily: A zircon tale from the basement of the Peloritani Mountains.* Gondwana Res., **22**, 855–865.

Zurbriggen R. (2015) - *Ordovician orogeny in the Alps: a reappraisal.* Int. J. Earth Sci., **104**, 335–350.

Zurbriggen R., Franz L. & Handy M.R. (1997) - *Pre-Variscan deformation, metamorphism and magmatism in the Strona-Ceneri Zone (southern Alps of northern Italy and southern Switzerland)*. Schweiz. Mineral. Petrogr. Mitt., **77**, 361-380.

Manuscript received 20 June 2019; accepted 23 September 2019; published online 09 October 2019;
editorial responsibility and handling by A. Renzulli